AD NUMBER
AD491186
CLASSIFICATION CHANGES
TO: unclassified
FROM: confidential
LIMITATION CHANGES
TO: Approved for public release, distribution unlimited
FROM: Distribution authorized to U.S. Gov't. agencies and their contractors; Administrative/Operational Use; 08 FEB 1960. Other requests shall be referred to Naval Ordnance Lab., White Oak, MD.
AUTHORITY
USNOL ltr, 29 Aug 1974; USNOL ltr, 29 Aug 1974

CONFIDENTIAL

NAVORD REPORT 5679

10

491186

AD No. 3

ASTIA FILE COPY

SUMMARY OF THE NOL INVESTIGATIONS TO DATE OF THE AERODYNAMIC CHARACTERISTICS OF THE NAVY LOW DRAG BOMB (U)

8 FEBRUARY 1960

U. S. NAVAL ORDNANCE LABORATORY

WHITE OAK, MARYLAND

CONFIDENTIAL

U. S. NAVAL ORDNANCE LABORATORY

WHITE OAK
SILVER SPRING, MARYLAND

To all holders of NAVORD Report 5679 — Change 1
Insert change; write on cover 'Change 1 inserted'
Approved by Commander, U.S. NOL — 1 page

October 1961 — By direction

This publication is changed as follows:

M_{ℓ_δ} slope of rolling moment due to fin cant

M_{ℓ_p} slope of roll damping moment

Figure 5 - arrow on roll direction is backward.

Figures 31 and 32 - Vertical scale should be 4.0, 8.0, 12.0, etc., not 0.04, 0.08, 0.12, etc.

Insert this change sheet between the cover and the title page of your copy.

CONFIDENTIAL
NAVORD Report 5679

Aerodynamics Research Report 11

SUMMARY OF THE NOL INVESTIGATIONS TO DATE OF THE AERODYNAMIC CHARACTERISTICS OF THE NAVY LOW DRAG BOMB

Prepared by

W. D. Piper
F. J. DeMeritte

ABSTRACT: This report summarizes the available aerodynamic data on the Navy Low Drag Bomb. The data were obtained from a series of investigations conducted by the Naval Ordnance Laboratory personnel in the NOL Supersonic Tunnel No. 1, the NOL Aerodynamics Range No. 1, the NOL Pressurized Ballistics Range No. 3, the David Taylor Model Basin 8 x 10 Foot Subsonic Wind Tunnel, and the Cornell Aeronautical Institute 3 x 4 Foot Transonic Wind Tunnel.

The aerodynamic data are presented as functions of angle of attack at Mach numbers of 0.80, 1.56, and 2.16 and as functions of Mach number for Mach numbers between 0.80 and 2.16.

U. S. NAVAL ORDNANCE LABORATORY
White Oak, Maryland

NAVORD Report 5679 8 February 1960

This is a summary report on wind-tunnel tests performed on the Navy Low Drag Bomb. These tests were performed at the request of the Bureau of Naval Weapons under Task Number 103-666/64045/02.

JOHN A. QUENSE', Acting
Captain, USN
Commander

R. KENNETH LOBB
By direction

CONTENTS

ILLUSTRATIONS

SUMMARY OF THE NOL INVESTIGATIONS TO DATE OF THE AERODYNAMIC CHARACTERISTICS OF THE NAVY LOW DRAG BOMB

INTRODUCTION

1. The Low Drag Bomb series consists of a 250 pound, a 500 pound, a 1000 pound, and a 2000 pound bomb of a shape originating from an external store developed by the Douglas Aircraft Company.

2. The Naval Ordnance Laboratory was directed by the Bureau of Naval Weapons to investigate the aerodynamic characteristics of the bomb in order to explain large pitching and yawing oscillations observed in its trajectory during full scale drop tests (reference (a)). Consequently, a series of tests were conducted by NOL in the NOL Pressurized Ballistics Range No. 3, the NOL Supersonic Tunnel No. 1, the David Taylor Model Basin 8 x 10 Foot Subsonic Wind Tunnel, and in the Cornell Aeronautical Institute 3 x 4 Foot Transonic Wind Tunnel. The results of most of these individual tests have already been published in the NAVORD Reports listed in references (b) through (l). This report summarizes the results obtained from the various tests on the Low Drag Bomb.

3. All of the data included in this report are for the basic Low Drag Bomb with 1.4 d fin span and 2° fin cant.

AERODYNAMIC SYMBOLS

A	reference area (maximum body diameter)
c.g.	center of gravity, 3.644 cal. forward from the base
C_N	normal force coefficient (F_N/qA)
$C_{\mathcal{O}}$	pitching moment coefficient ($M_{\mathcal{O}}/qAd$)
$C_{\mathcal{O}_\alpha}$	slope of pitching moment coefficient curve $\left(\frac{dC_{\mathcal{O}}}{d\alpha}\right)$
C_y	side force coefficient (F_y/qA)
C_{y_m}	Magnus force coefficient (F_{y_p}/qA)
C_{y_p}	Magnus force slope coefficient $\left(\partial C_{y_p}/\partial\left(\frac{pd}{2V}\right)\right)$
C_ℓ	rolling moment coefficient (M_ℓ/qAd)
$C_{\ell_{\gamma_\alpha}}$	induced rolling moment coefficient ($M_{\ell_{\gamma_\alpha}}/qAd$)

$C_{m_q} + C_{m_{\dot{\alpha}}}$	pitch damping coefficient $\frac{16\mu}{\pi\rho V d^4}$
C_{ℓ_δ}	rolling moment coefficient due to fin cant $\frac{M_{\ell_\delta}}{qAd}$
C_{ℓ_p}	roll damping moment coefficient $\frac{M_{\ell_p}}{p} \cdot \frac{1}{qAd} \cdot \frac{2V}{d}$
C_ψ	yawing moment coefficient (M_ψ/qAd)
C_{ψ_m}	Magnus moment coefficient (M_{ψ_p}/qAd)
C_{ψ_p}	Magnus moment slope coefficient $(\partial C_{\psi_p}/\partial)(pd/2V)$
d	reference diameter (model maximum diameter = cal.)
F_N	normal force (lbs)
F_y	side force (lbs)
F_{y_p}	Magnus force (lbs)
I	axial moment of inertia (slugs-ft^2)
M	Mach number
M_Θ	pitching moment (in-lbs)
M_ℓ	rolling moment (in-lbs)
$M_{\ell_{\gamma_\alpha}}$	rolling moment induced by roll orientation and angle of attack (in-lbs)
M_{ℓ_δ}	rolling moment due to fin cant (in-lbs)
M_{ℓ_p}	roll damping moment (in-lbs)
M_ψ	yawing moment (in-lbs)
M_{ψ_p}	Magnus moment (in-lbs)
p	spin rate (rad/sec or RPM)
q	dynamic pressure (psi)
V	velocity (fps)
Re	Reynolds Number (based on model length)
α	angle of attack (deg)
δ	angle of fin cant (deg)
γ	angle of roll of fins (rad)
ϕ	angle of roll of the model (deg)(in this report $\gamma = \phi$)
ψ	angle of yaw (deg)
μ	damping constant (ft-lb-sec)/rad)

MODELS, TEST TECHNIQUES, AND DATA REDUCTION

4. Because it was necessary to use models of different sizes in each of the different wind tunnels, the model dimensions are shown in Figure 1 in units of maximum body diameter.

5. The tail cones of the wind-tunnel static and Magnus force models were removed as shown in Figures 1 and 2 in order to mount the models on an internal strain-gage type balance. The static test data taken at NOL were recorded and reduced as described in references (m) and (n) respectively.

6. The wind-tunnel Magnus data were obtained at the David Taylor Model Basin and the Cornell Aeronautical Laboratory using internal strain-gage type balances designed and constructed by NOL especially for the Magnus force testing. The Magnus force data reduction and test technique are described in reference (o).

7. The model for the damping tests was dynamically balanced about the scaled full scale center of gravity. A shaft whose axis was normal to the longitudinal axis of the model was passed through the center of gravity and was attached to the model by means of precision ball bearings of very low frictional torque. The model was thus able to rotate in the pitch plane about a transverse axis which passes through the center of gravity. Figure 3 shows the damping model mounted on its shaft. The data were obtained from high speed motion pictures taken of the model during its damping oscillations. The technique of reducing the damping data is described in detail in reference (b).

8. The models tested in the Aerodynamics Range No. 1 and the Pressure Ballistics Range No. 3 were launched using a sabot as shown in Figure 4. In brief, the ballistics range data were obtained by firing a model down the range and fitting the data obtained from spark shadowgraphs taken at successive stations along the range to the assumed equations of motion. The complete data reduction technique is described in reference (p).

9. The coordinate axes and sign convention are shown in Figure 5 at a model orientation of $\phi = 0$ degrees ($\gamma = 0$ degrees). The fins are in the vertical and horizontal planes and the lugs are rotated clockwise (positive roll) 45 degrees from the vertical.

DISCUSSION

10. All of the data presented in this report are reduced to coefficient form and whenever possible are presented by curves both as a function of angle of attack and as a function of Mach number. In some of the curves where Mach number is the parameter it was necessary to extrapolate between rather large gaps in Mach numbers where no data were available. Consequently, the coefficients are presented as a function of Mach number only to indicate the trend due to Mach number and not necessarily as explicit point values. The data were obtained over an angle of attack range from 0 to 24 degrees except at Mach number 0.8. At the Mach number of 0.8 the static test data were obtained over an angle of attack range of 0 to 32 degrees. The pitch damping coefficients were obtained at an angle of attack of 40 degrees. The Magnus force and moment data were determined up to an angle of attack of 20 degrees. The plots of coefficient versus Mach number show data in the subsonic Mach number range where possible up to angles of attack of 40 degrees. These data were required for computer studies at the Naval Weapons Laboratory. The data were obtained by extrapolating the Mach number 0.8 data to 40 degrees angle of attack. It was not possible in every case to extrapolate the data to 40 degrees with any degree of certainty. Data have been extrapolated, in nearly every case, to the limit, and the data shown beyond the last test point are included to show possible trends only.

11. During most of the tests reported in references (b) through (l) the basic configuration was tested over at least a limited range of parameters as a reference configuration. In addition certain of the coefficients are obtained as a by-product of other tests. For example, the pitching moment coefficients have been obtained from static stability tests in the wind tunnels, shots fired in the firing ranges, pitch damping tests, and Magnus tests where pitching moments as well as Magnus moments are obtained. These tests sometimes give small variations to the coefficients. The data presented in this report represent what is considered to be the best estimate of the coefficients obtained for the Low Drag Bomb.

12. Because of the variation in Reynolds number due to the different model sizes and test conditions, the Reynolds numbers are not given for any of the data except the Magnus coefficients. The close agreement between data obtained at different Reynolds numbers using the various test techniques indicates the Reynolds number effect will be small except on the Magnus characteristics.

13. The normal force coefficients (C_N) are shown in Figures 6 through 8 as a function of angle of attack and in Figures 9 through 11 as a function of Mach number.

14. The pitching moment coefficients (C_Q) are presented as a function of angle of attack in Figures 12 through 14 and as a function of Mach number in Figures 15 through 17. It should be noted that as the Mach number increases (supersonic speeds) there is a rapid and almost linear decrease in the slope of the pitching moment coefficient. This trend toward static instability is quite evident in Figure 18 where the slope of pitching moment coefficient (C_{Q_α}) at α = 0 degrees is shown as a function of Mach number. It is evident that if the trend continues the bomb will be statically unstable at small angles of attack at Mach numbers above 2.25.

15. The side force coefficient (C_y) data are presented in Figures 19 through 21 as a function of angle of attack while Figures 22 through 24 present the side force coefficient vs. Mach number.

16. The yawing moment coefficient (C_ψ) data are shown vs. angle of attack in Figures 25 through 27 and vs. Mach number in Figures 28 through 30.

17. The Magnus force and moment coefficients (C_{y_p}, C_{ψ_p}) are shown versus angle of attack in Figures 31 and 32. The Magnus coefficients (C_{y_m} and C_{ψ_m}) are shown versus Mach number in Figure 33. These data (C_{y_m} and C_{ψ_m}) do not include the spin parameter pd/2V. For these data, p = 2000 RPM and d = 3.0 inches. No Magnus data exist at Mach numbers above 1.25; however, the trend of the data indicates that the Magnus coefficients are very small at the higher Mach numbers. The majority of the data was taken at a Reynolds number of four million based on body length. However, the data at Mach number 0.6 were obtained at a Reynolds number of six million. The Magnus force is generally in the same order of magnitude as the side force and is about in the order of 10 to 20 percent of the normal force.

18. The pitch damping moment coefficient ($C_{m_q} + C_{m_{\dot{\alpha}}}$) data are shown for fin orientations of 0^o and -45^o as functions of angle of attack, with the Mach number as a parameter, in Figures 34 and 35, respectively. The pitch damping coefficients are shown as function of Mach number in Figure 36 with the angle of attack as parameter.

19. The roll damping moment coefficient (C_{ℓ_p}) data are presented versus angle of attack in Figure 37 for a Mach number of 0.8 and as a function of Mach number at zero degree angle of attack in Figure 38.

20. The rolling moment coefficient due to fin cant (C_{ℓ_δ}) is shown in Figure 39 as a function of angle of attack for Mach number of 0.8 and as a function of Mach number in Figure 38 at zero angle of attack.

21. The induced rolling moment coefficient ($C_{\ell_{\gamma_\alpha}}$) is the rolling moment coefficient due to angle of attack and asymmetrical fin orientation. The induced rolling moment coefficient is presented as a function of angle of attack in Figures 40 through 42 and as a function of Mach number in Figures 43 through 45.

22. The drag coefficient at zero angle of attack (C_{D_o}) versus Mach number is shown in Figure 46. These data were obtained in the firing range on models of the 1000 pound Low Drag Bomb with scaled fin thickness. These data are from reference (j).

SUMMARY

23. This report presents a summary of the available aerodynamic coefficient data on the Low Drag Bomb in a number of NAVORD Reports. Some of these coefficients such as the yawing moment, side force, or Magnus force and Magnus moment are quite small and are very difficult to measure accurately. These data are the coefficients transmitted to the Naval Weapons Laboratory for computing trajectories of the Low Drag Bomb.

REFERENCES

(a) Madden, J. J., "Separation and Free-Flight Tests of 250 pound Mk 81 and 500 pound Mk 82 Low Drag General Purpose Bombs Released from A3D-1 Aircraft," NPG Report 1551, Conf., (1957)
(b) Shantz, I., and Groves, R. T., "Subsonic Damping in Pitch Measurements of the EX-10, EX-30, and 6" Test Vehicle," NAVORD Report 4025, Conf., (1958)
(c) Long, J. E., "Free-Flight Investigation of the Stability and Drag of the EX-10 General Purpose Bomb," NAVORD Report 2916, Conf., (1953)
(d) Long, J. E., "Low-Yaw Data on the Low Drag Bomb (EX-010) at Transonic Speeds ($0.7<M<1.4$)," NAVORD Report 4227, Conf., (1956)
(e) Long, J. E., "Roll Coefficients for the Low Drag Bomb (EX-10) in the Transonic Velocity Region ($0.65<M<1.31$)," NAVORD Report 4389, Conf., (1956)
(f) Gauzza, H. J., "Aeroballistic Investigation of the EX-10 Bomb at Subsonic Speeds," NAVORD Report 2814, Conf., (1953)
(g) Greene, J. E., "Static Stability and Magnus Characteristics of a Low Drag Bomb at Low Subsonic Speeds," NAVORD Report 4112, Conf., (1956)
(h) Greene, J. E., "Static Stability and Magnus Characteristics of the U. S. Navy 1000 Pound Low Drag Bomb at Transonic Speeds," NAVORD Report 4329, Conf., (1957)
(i) Piper, W. D., "Static Stability Characteristics of the EX-10 Low Drag Bomb," NAVORD Report 4503, Conf., (1958)
(j) Crogan, L. E., "Drag and Roll Coefficients at Subsonic to Supersonic Velocities of 1/7-Scale Free-Flight Models of the 1000 Pound Low Drag Bomb (EX-10)," NAVORD Report 6661, Unclass.
(k) DeMeritte, F. J., Gauzza, H., "Wind-Tunnel Investigation of Various Configurational Modifications of the Low Drag Bomb," NAVORD Report 4053, Conf., (1959)
(l) DeMeritte, F. J., Gauzza, H., Shantz, I., "Miscellaneous Wind-Tunnel Tests on the Low Drag Bomb," NAVORD Report 5702, Unclass., (1959)
(m) Shantz, I., Gilbert, B. D., and White, C. E., "NOL Wind Tunnel Internal Strain-Gage Balance System," NAVORD Report 2972, 1953
(n) Gilbert, B. D., "Automatic Data Processing System (ADAPS) for the Supersonic Wind Tunnels," NAVORD Report 2813, (1953)
(o) Luchuk, W., and Sparks, W., "Wind-Tunnel Magnus Characteristics of the 7-Caliber Army-Navy Spinner Rocket," NAVORD Report 3813, Conf., (1954)
(p) Murphy, C. H., "Data Reduction for the Free-Flight Spark Ranges, BRL Report 900, (1954)

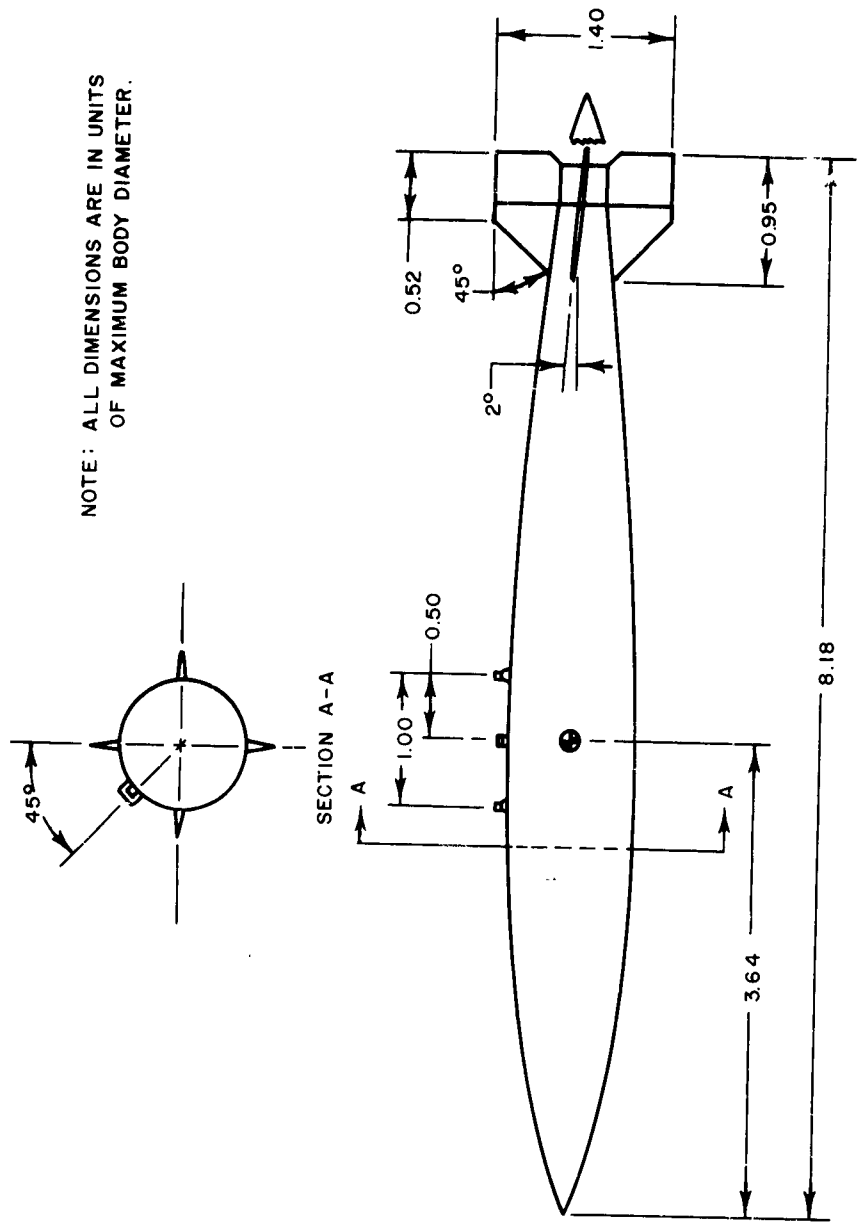

FIG. I U.S. NAVY GENERAL PURPOSE LOW DRAG BOMB

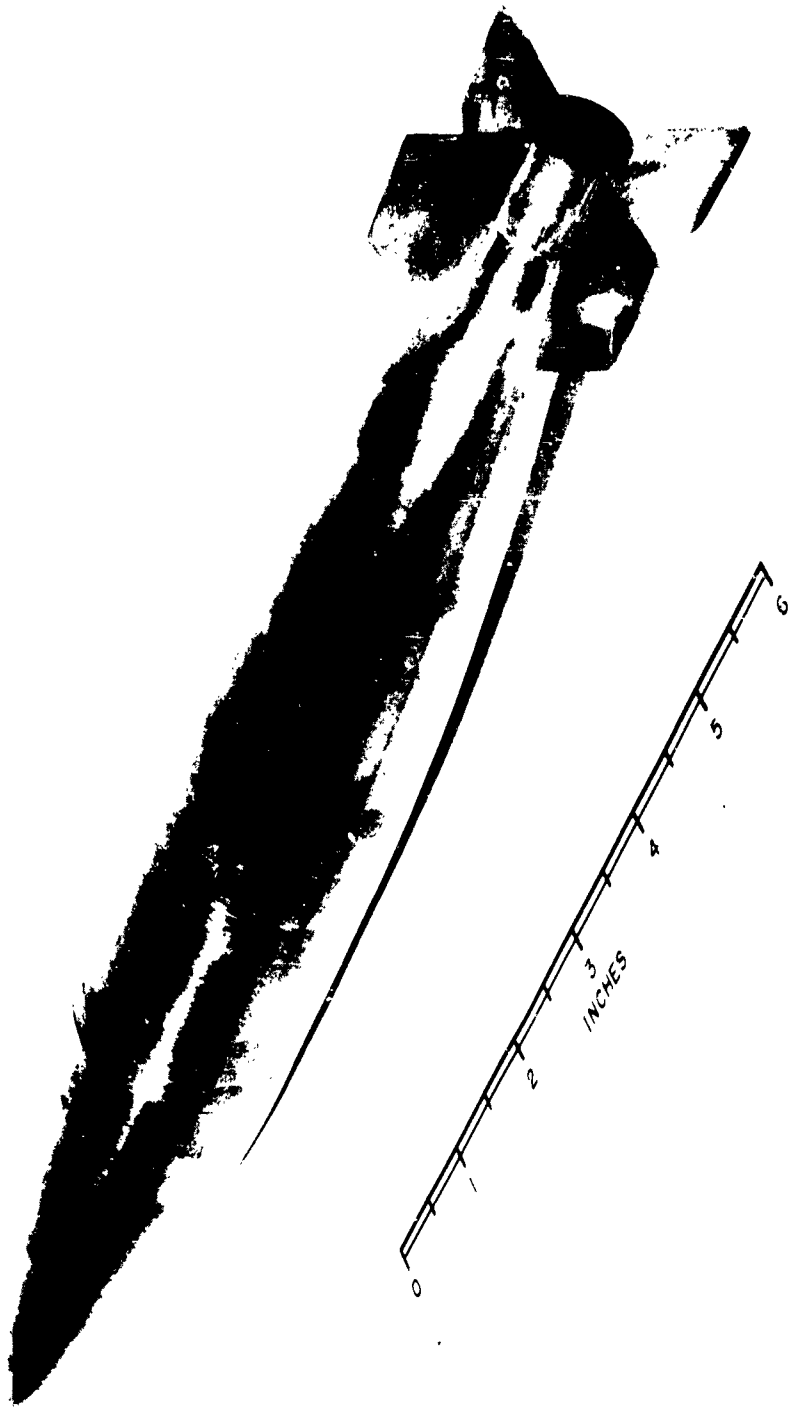

FIG. 2 WIND TUNNEL STATIC MODEL

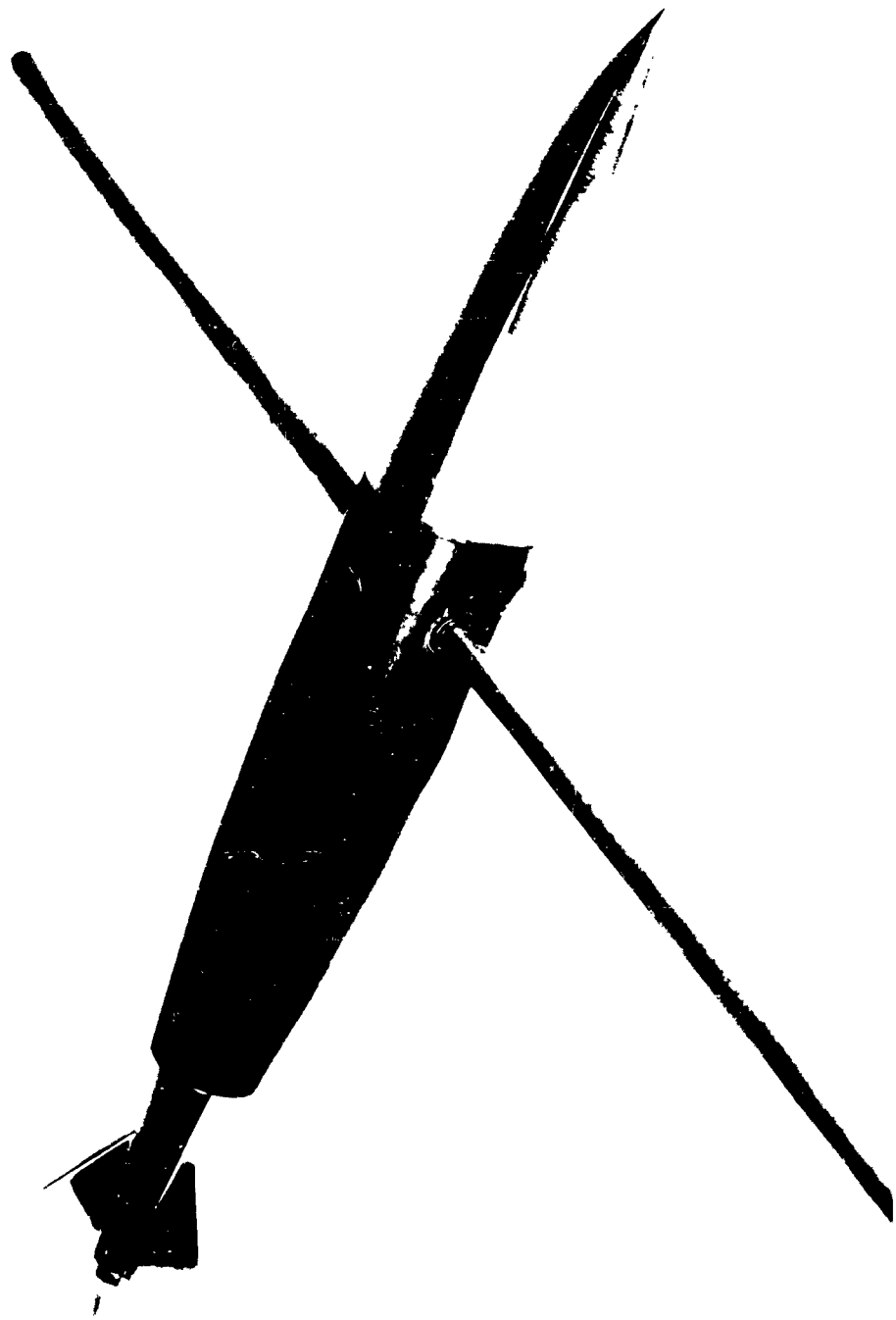

FIG. 3 WIND TUNNEL DAMPING MODEL

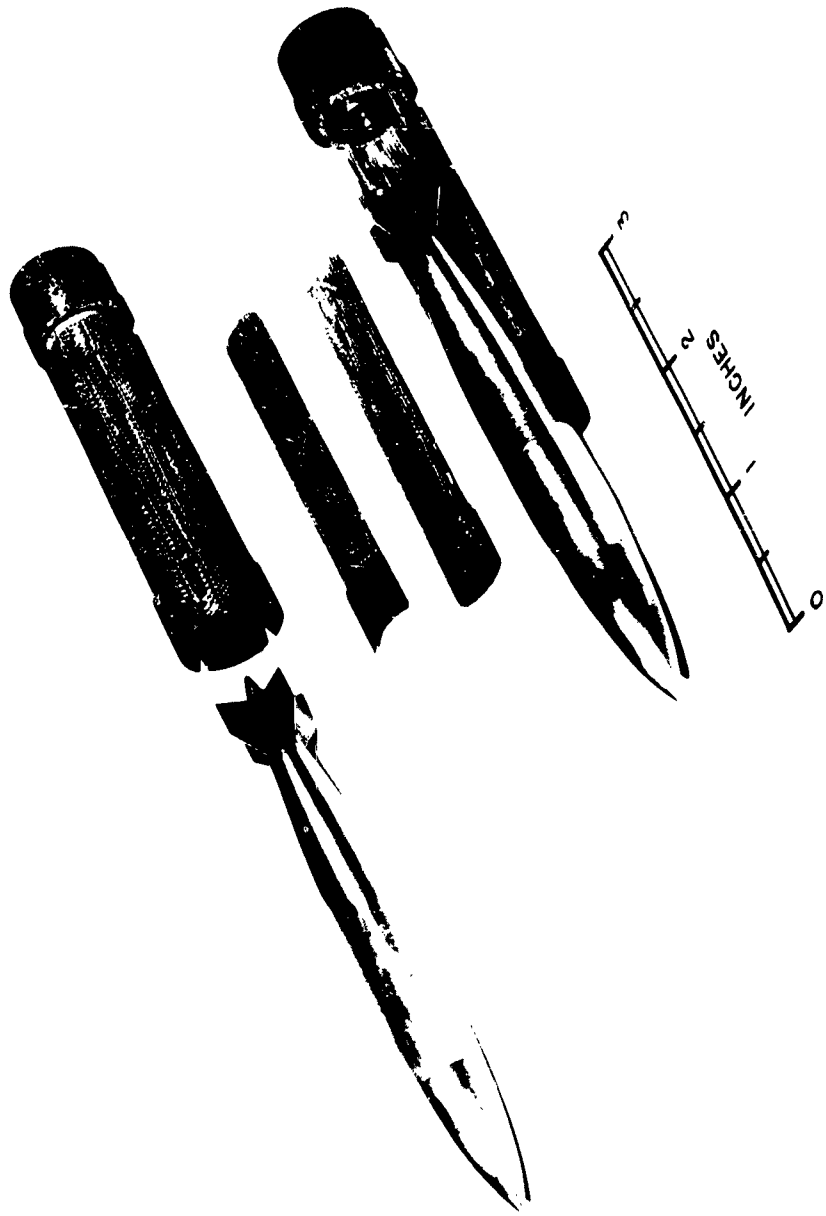

FIG. 4 RANGE MODEL AND LAUNCHING SABOT

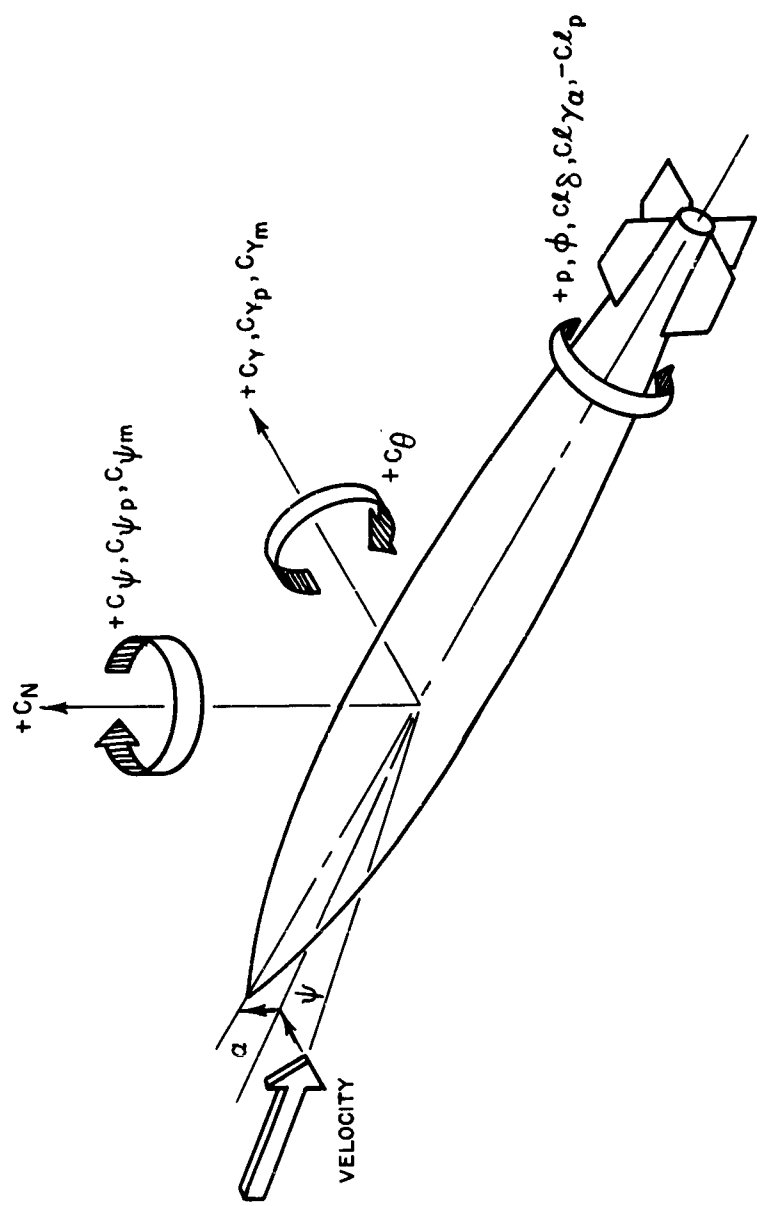

FIG.5 COORDINATE AXES AND SIGN CONVENTION

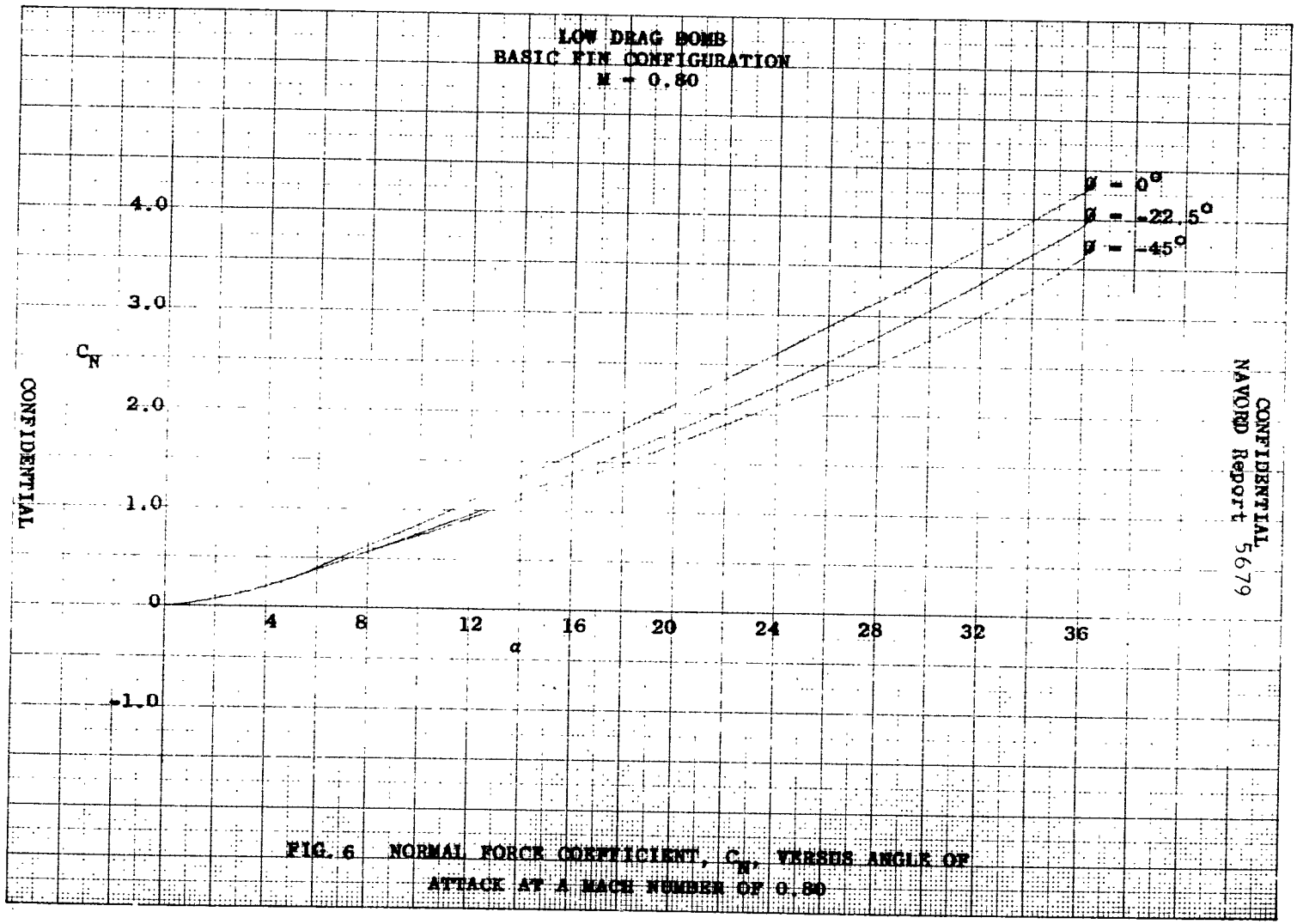

FIG. 6 NORMAL FORCE COEFFICIENT, C_N, VERSUS ANGLE OF ATTACK AT A MACH NUMBER OF 0.80

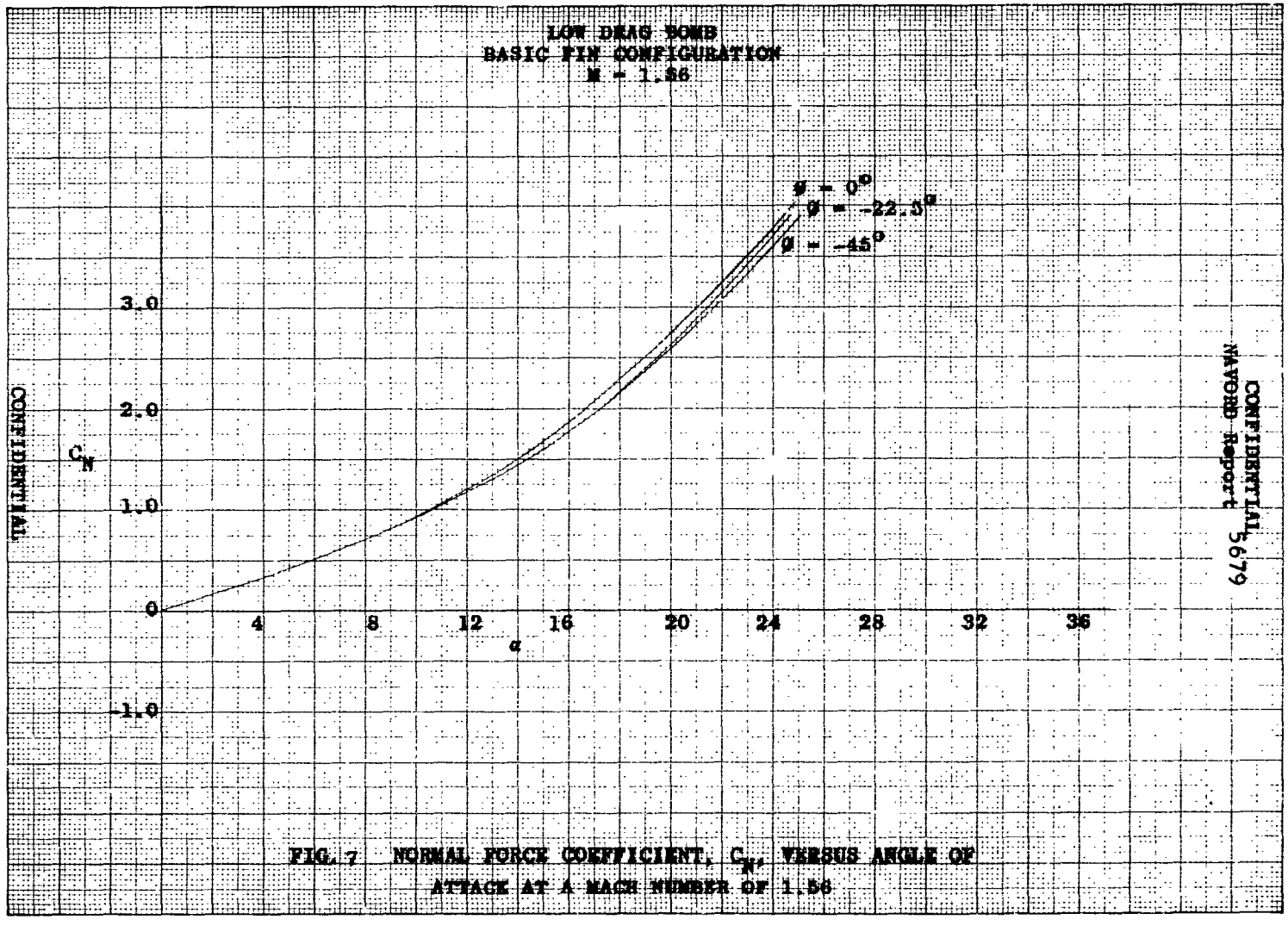

FIG. 7 NORMAL FORCE COEFFICIENT, C_N, VERSUS ANGLE OF ATTACK AT A MACH NUMBER OF 1.56

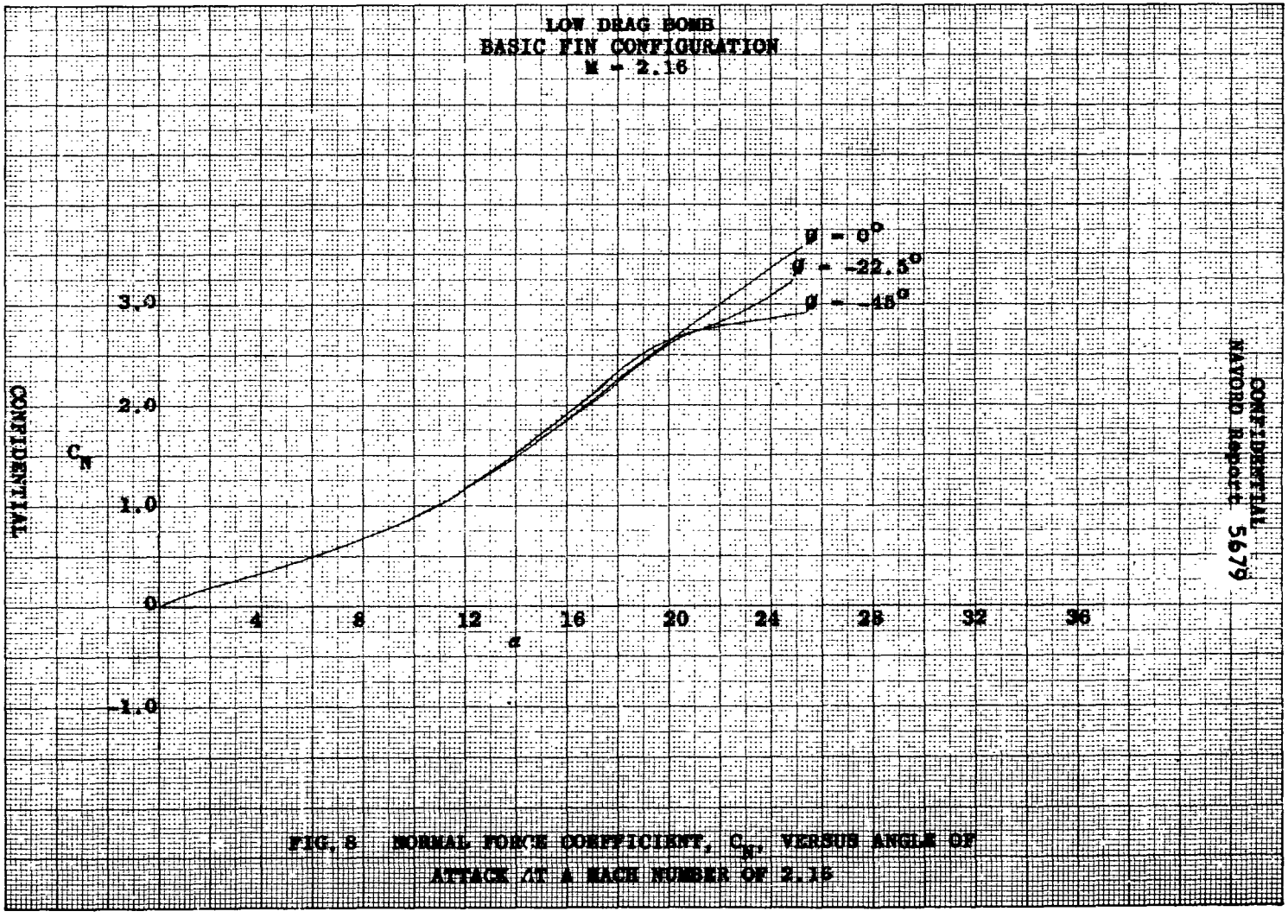

FIG. 8 NORMAL FORCE COEFFICIENT, C_N, VERSUS ANGLE OF ATTACK AT A MACH NUMBER OF 2.16

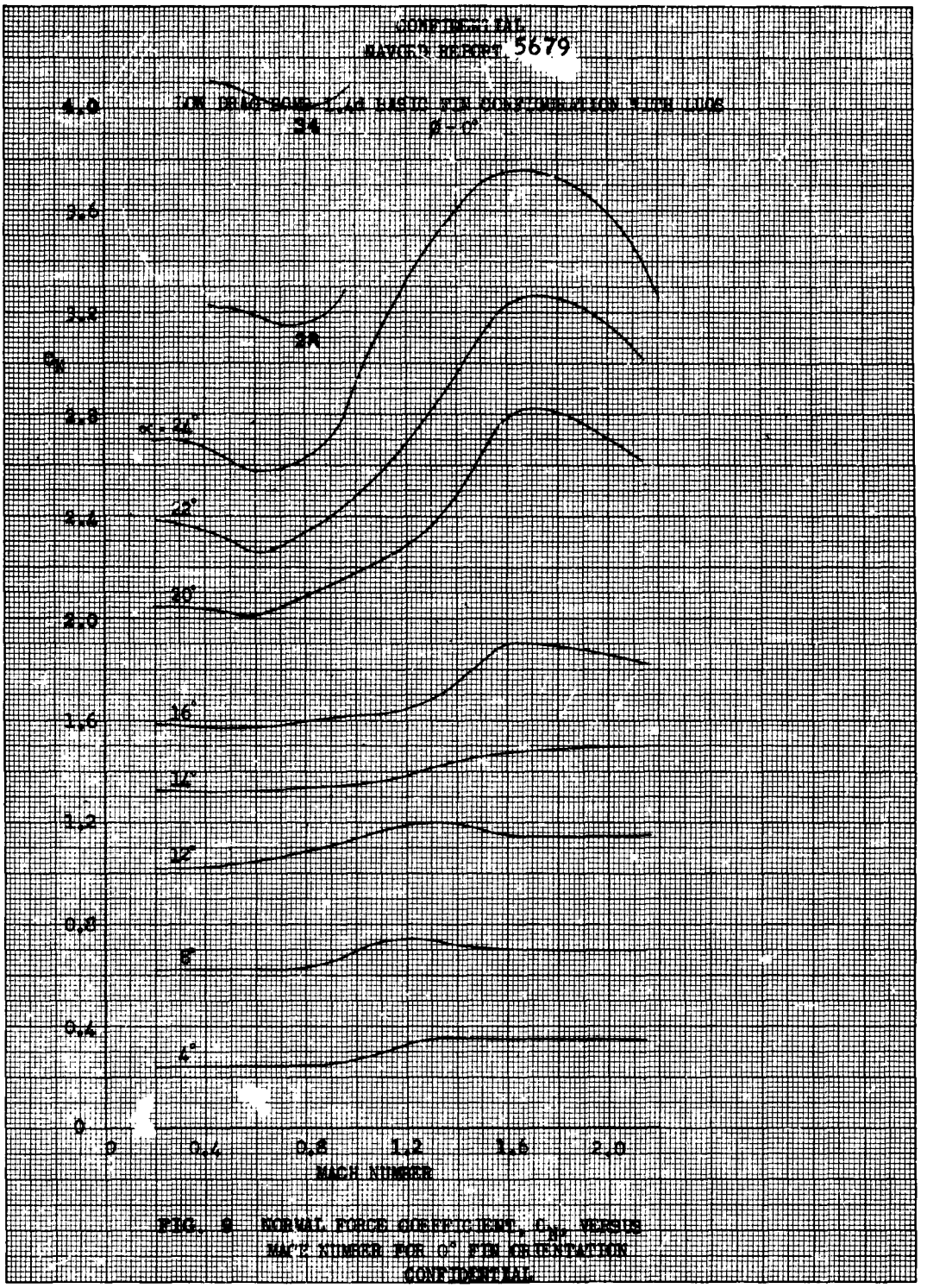

FIG. 8 NORMAL FORCE COEFFICIENT, C_{N_α} VERSUS MACH NUMBER FOR 0° FIN ORIENTATION

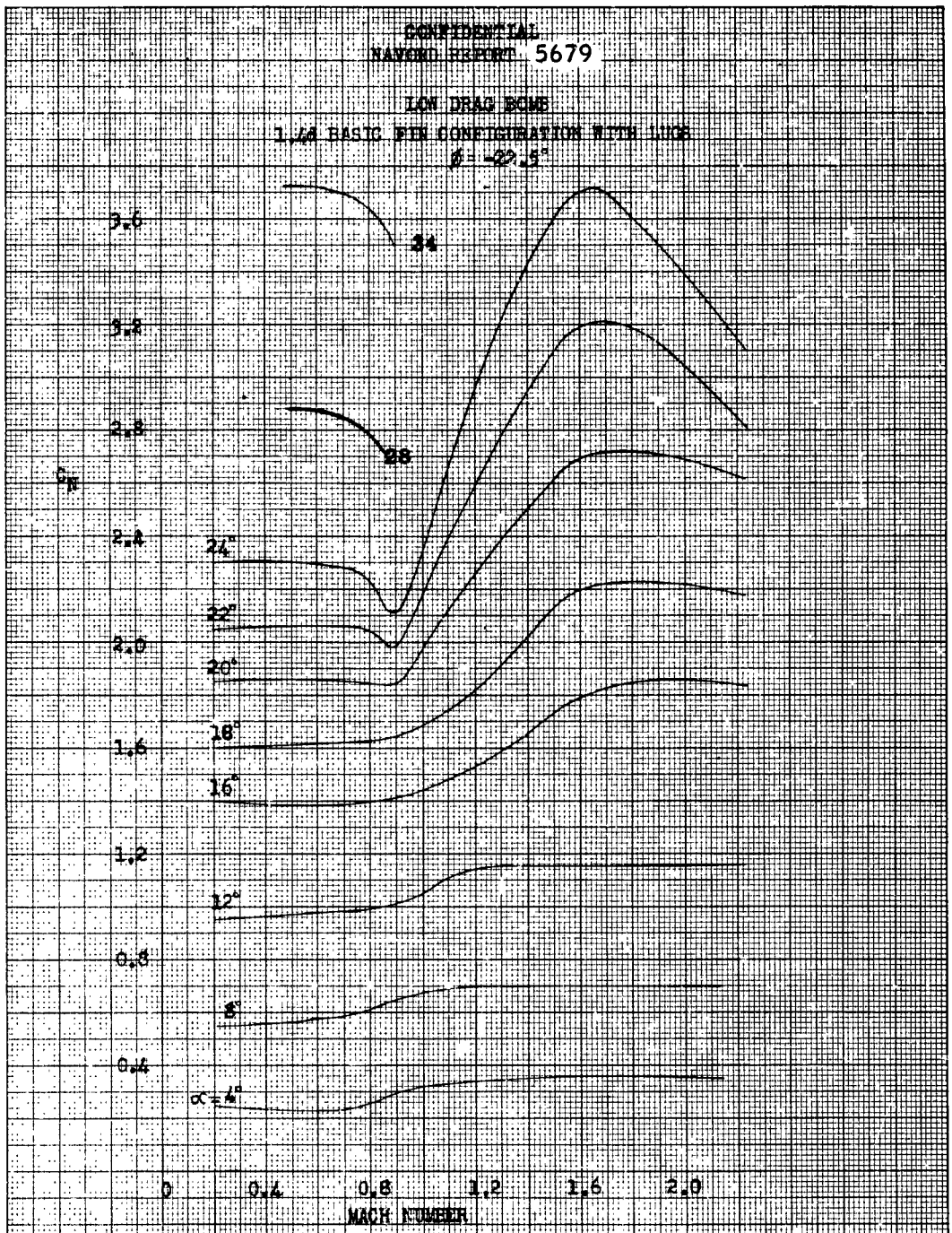

FIG. 10 NORMAL FORCE COEFFICIENT, C_N, VERSUS MACH NUMBER FOR -22.5° FIN ORIENTATION

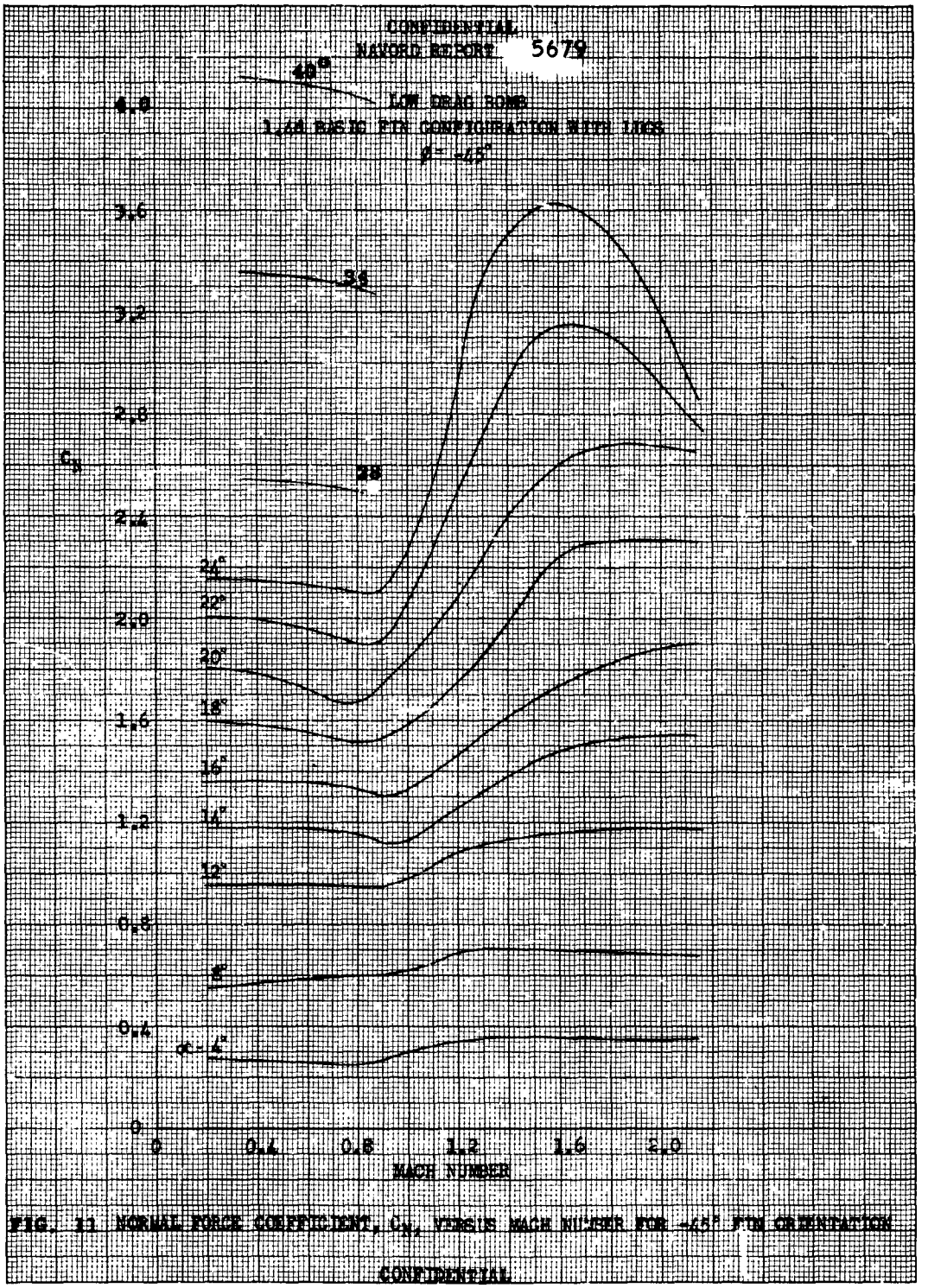

FIG. 11 NORMAL FORCE COEFFICIENT, C_{N_α} VERSUS MACH NUMBER FOR -45° FIN ORIENTATION

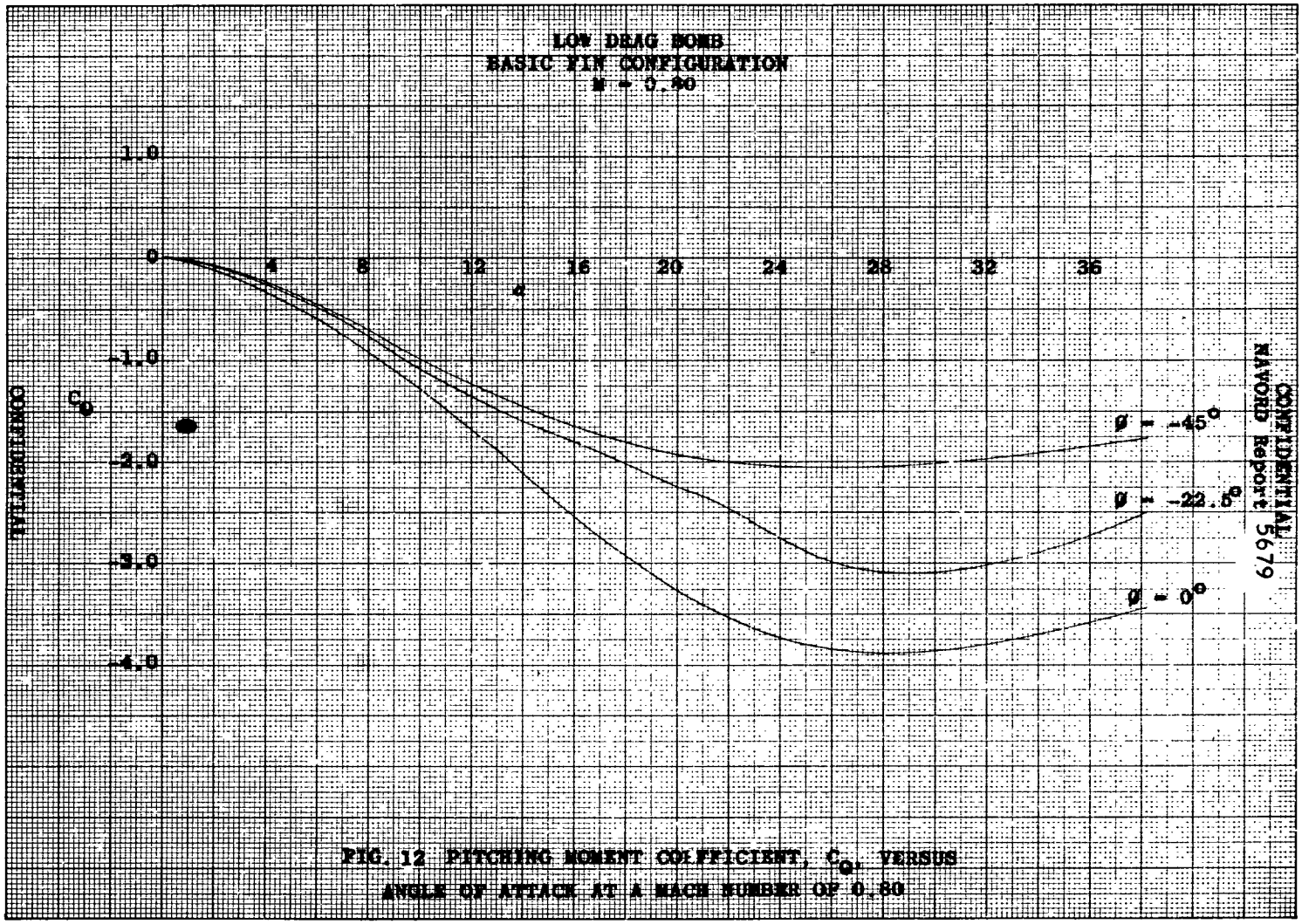

FIG. 12 PITCHING MOMENT COEFFICIENT, C_Q, VERSUS ANGLE OF ATTACK AT A MACH NUMBER OF 0.80

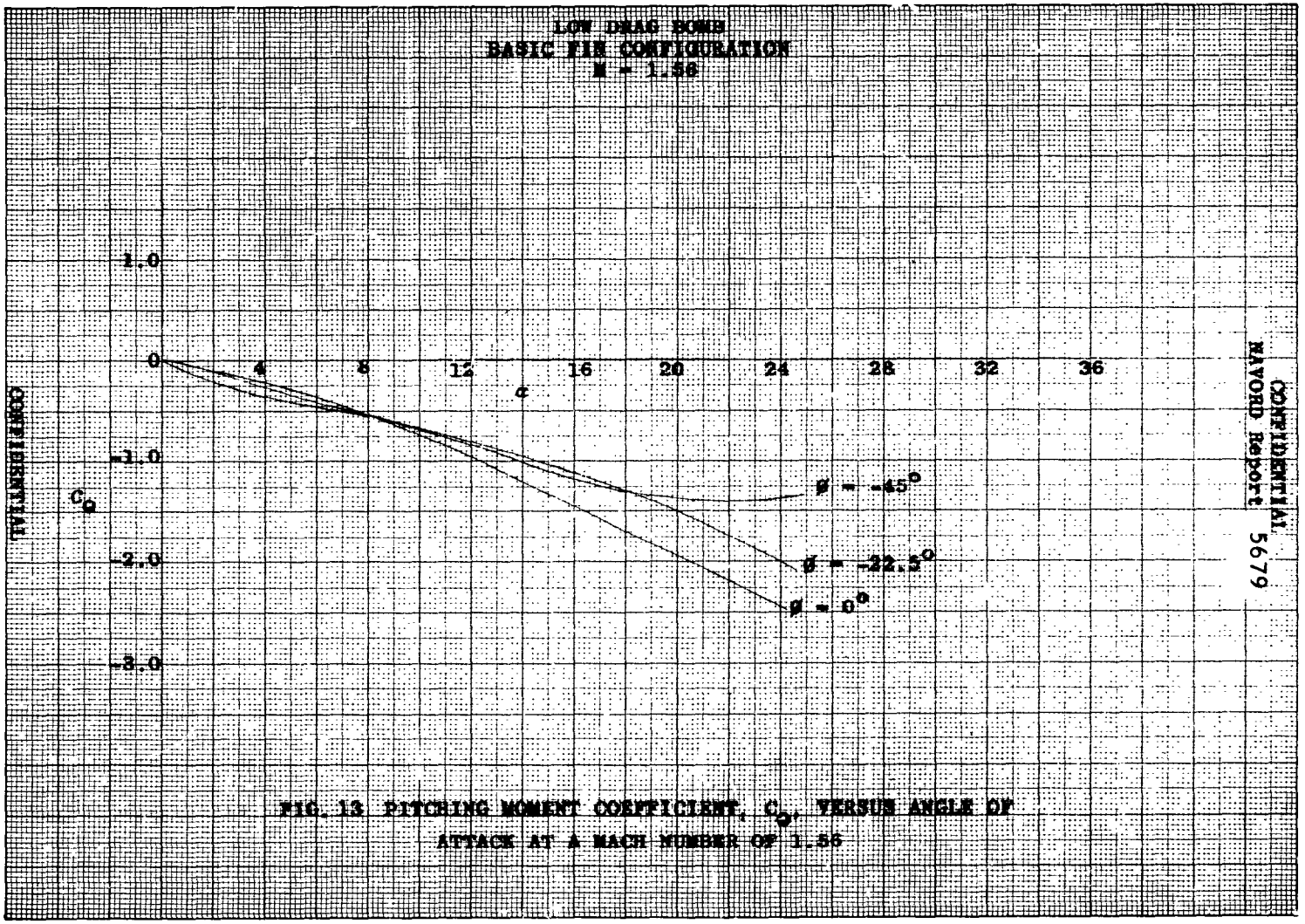

FIG. 13 PITCHING MOMENT COEFFICIENT, $C_{\mathcal{Q}}$, VERSUS ANGLE OF ATTACK AT A MACH NUMBER OF 1.56

FIG. 14 PITCHING MOMENT COEFFICIENT, C_m, VERSUS ANGLE OF ATTACK AT A MACH NUMBER OF 2.16

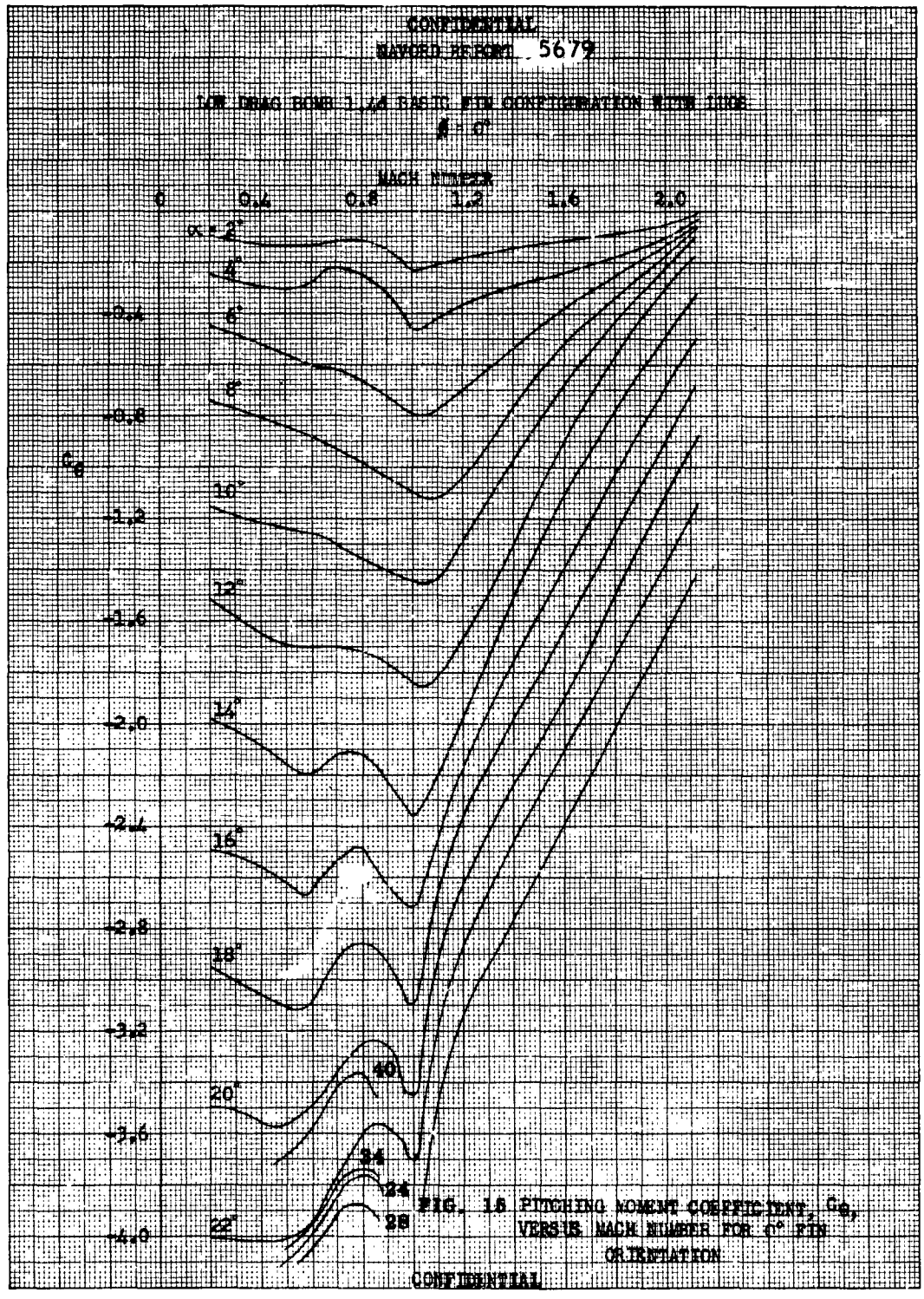

FIG. 16 PITCHING MOMENT COEFFICIENT, C_{m_0}, VERSUS MACH NUMBER FOR 0° FIN ORIENTATION

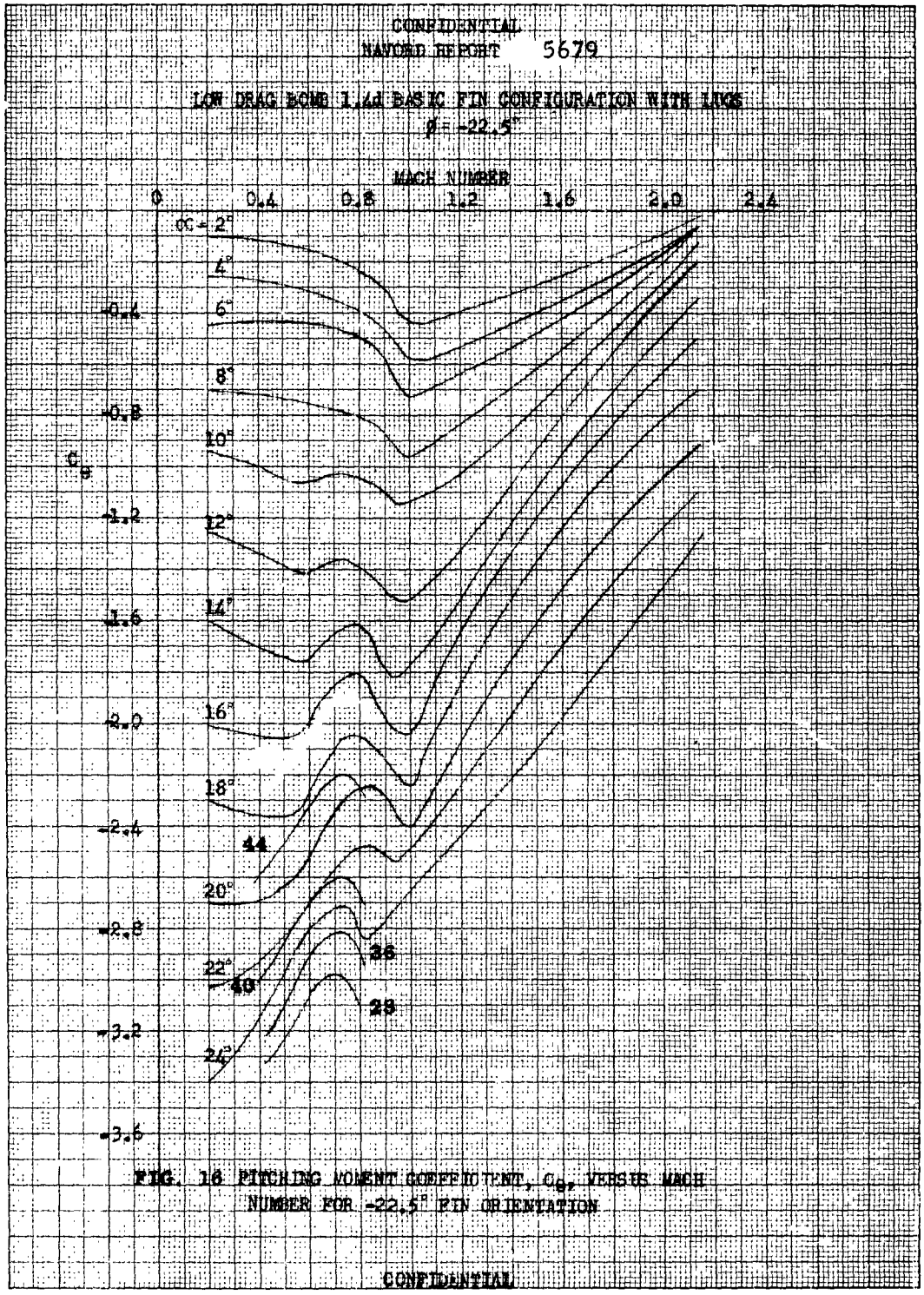

FIG. 16 PITCHING MOMENT COEFFICIENT, C_m, VERSUS MACH NUMBER FOR -22.5° FIN ORIENTATION

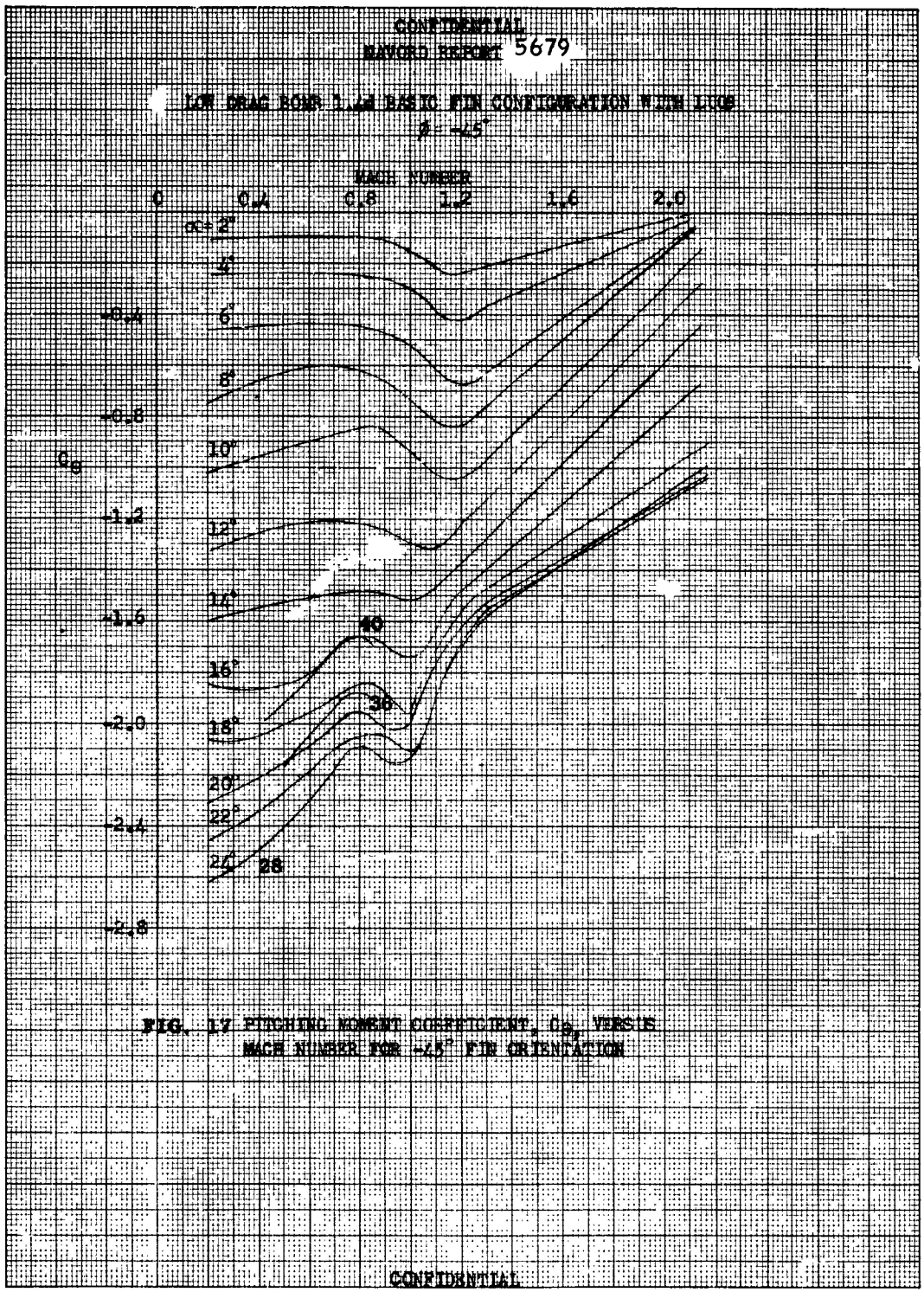

FIG. 17 PITCHING MOMENT COEFFICIENT, C_{B_β} VERSUS MACH NUMBER FOR -45° FIN ORIENTATION

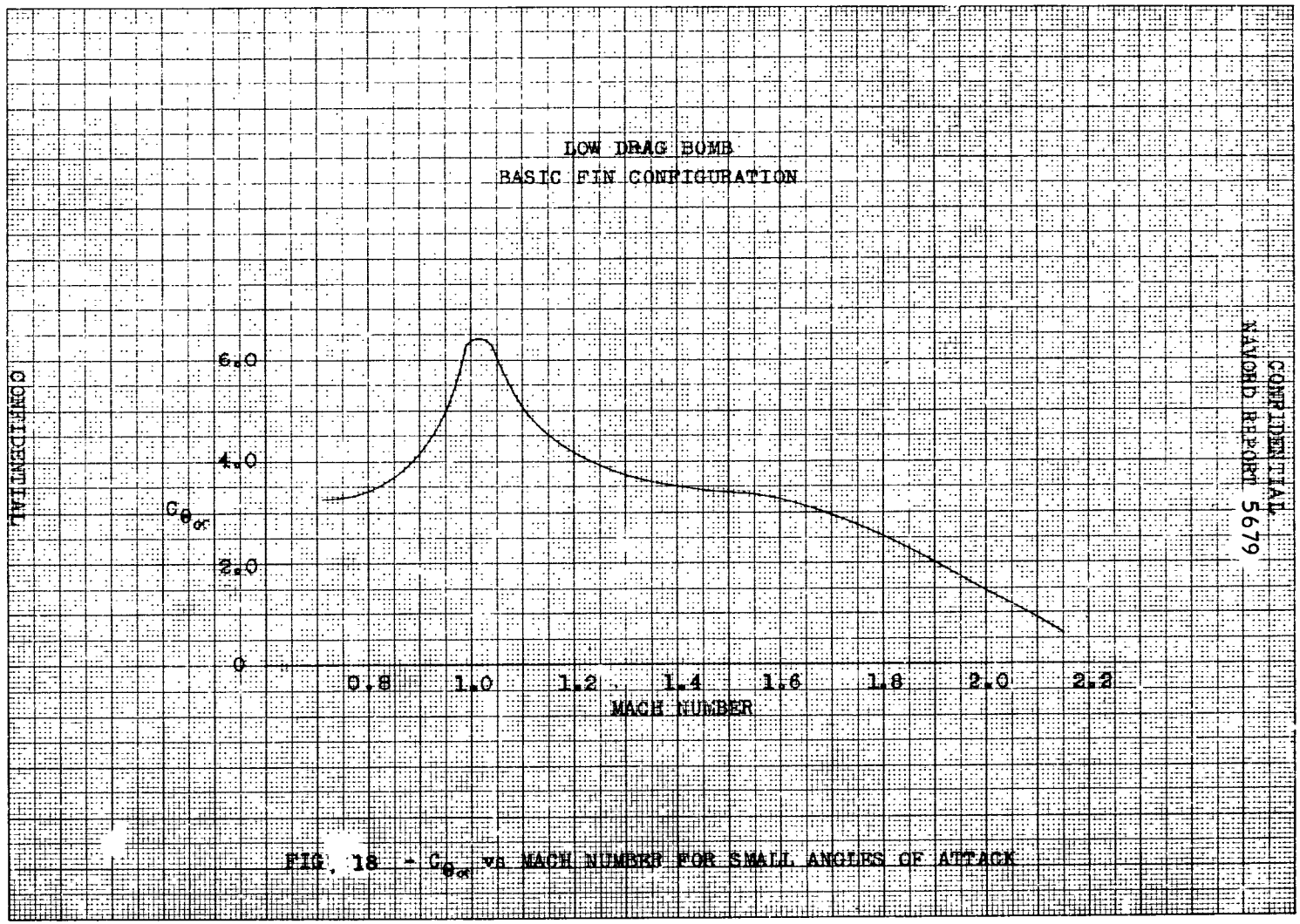

FIG. 18 - C_{θ_α} vs MACH NUMBER FOR SMALL ANGLES OF ATTACK

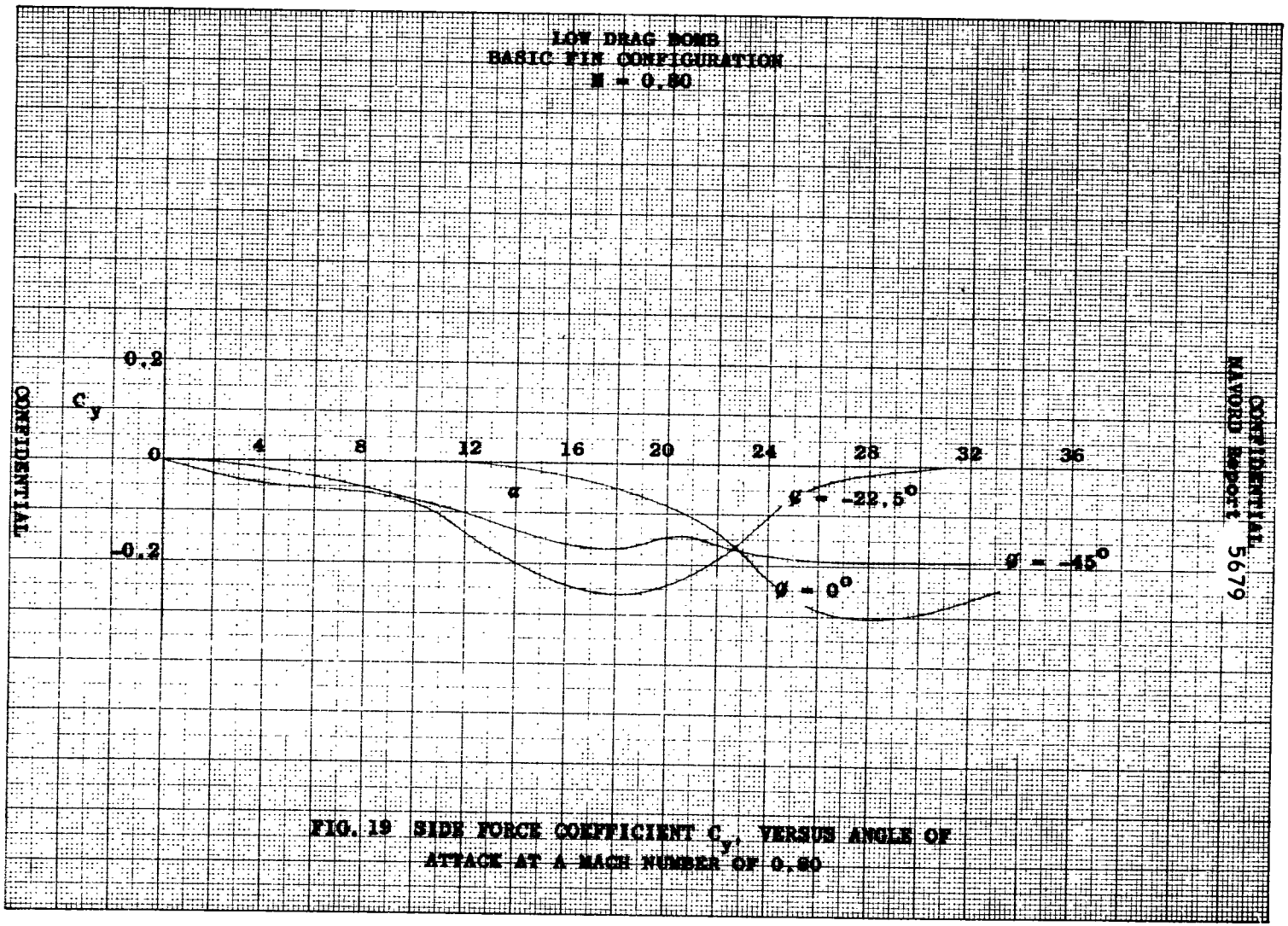

FIG. 19 SIDE FORCE COEFFICIENT C_y, VERSUS ANGLE OF ATTACK AT A MACH NUMBER OF 0.80

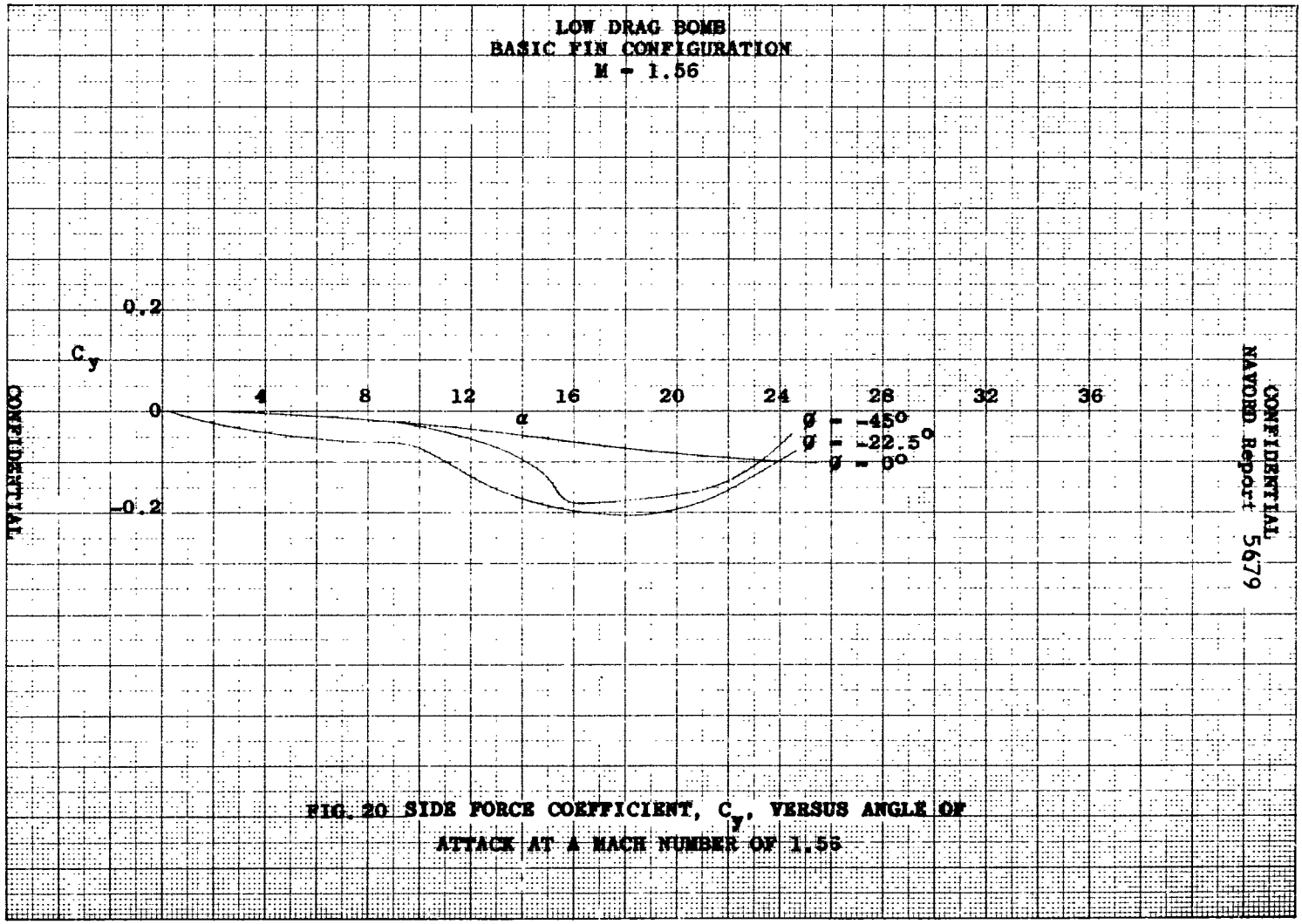

FIG. 20 SIDE FORCE COEFFICIENT, C_y, VERSUS ANGLE OF ATTACK AT A MACH NUMBER OF 1.56

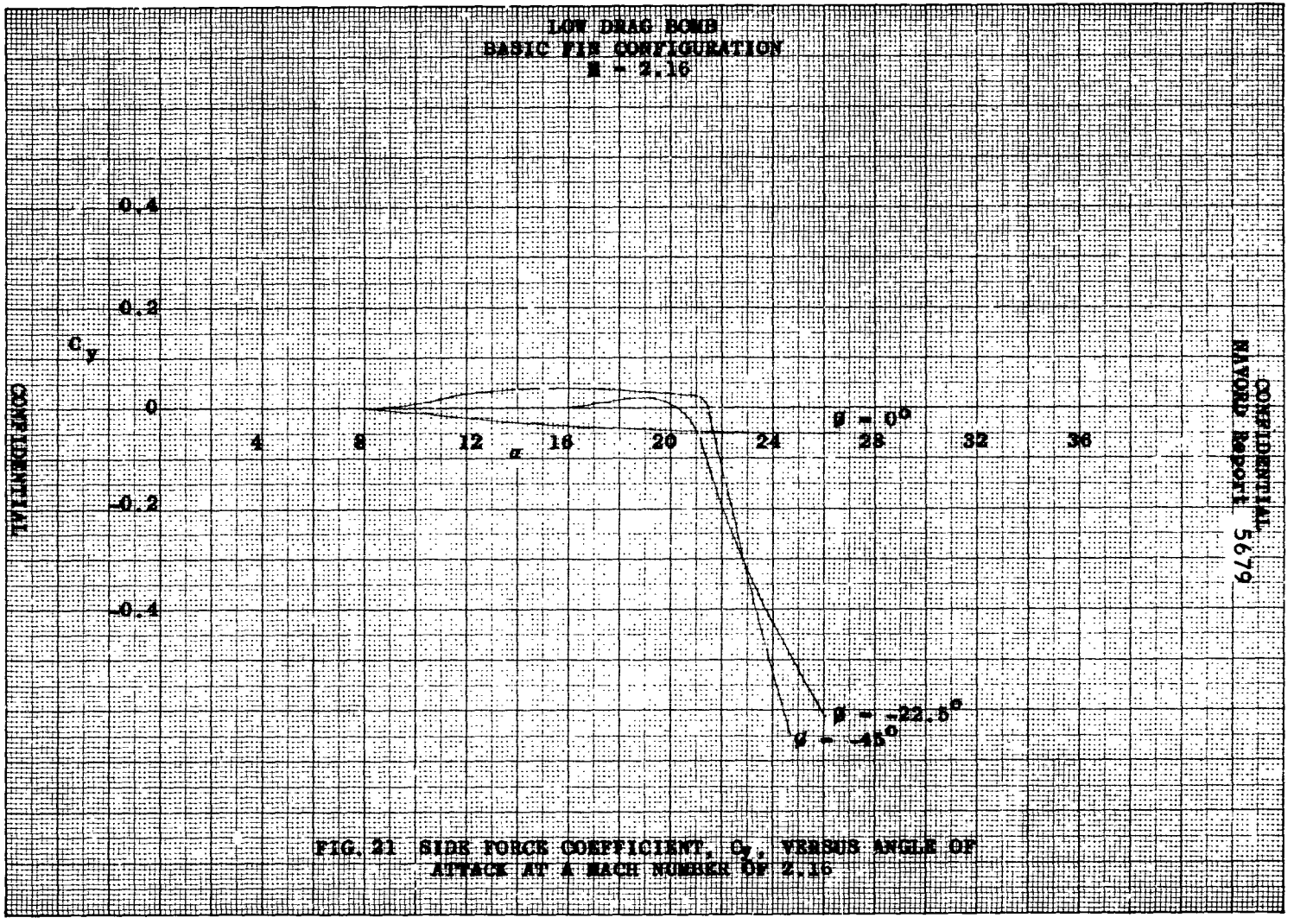

FIG. 21 SIDE FORCE COEFFICIENT, C_y, VERSUS ANGLE OF ATTACK AT A MACH NUMBER OF 2.16

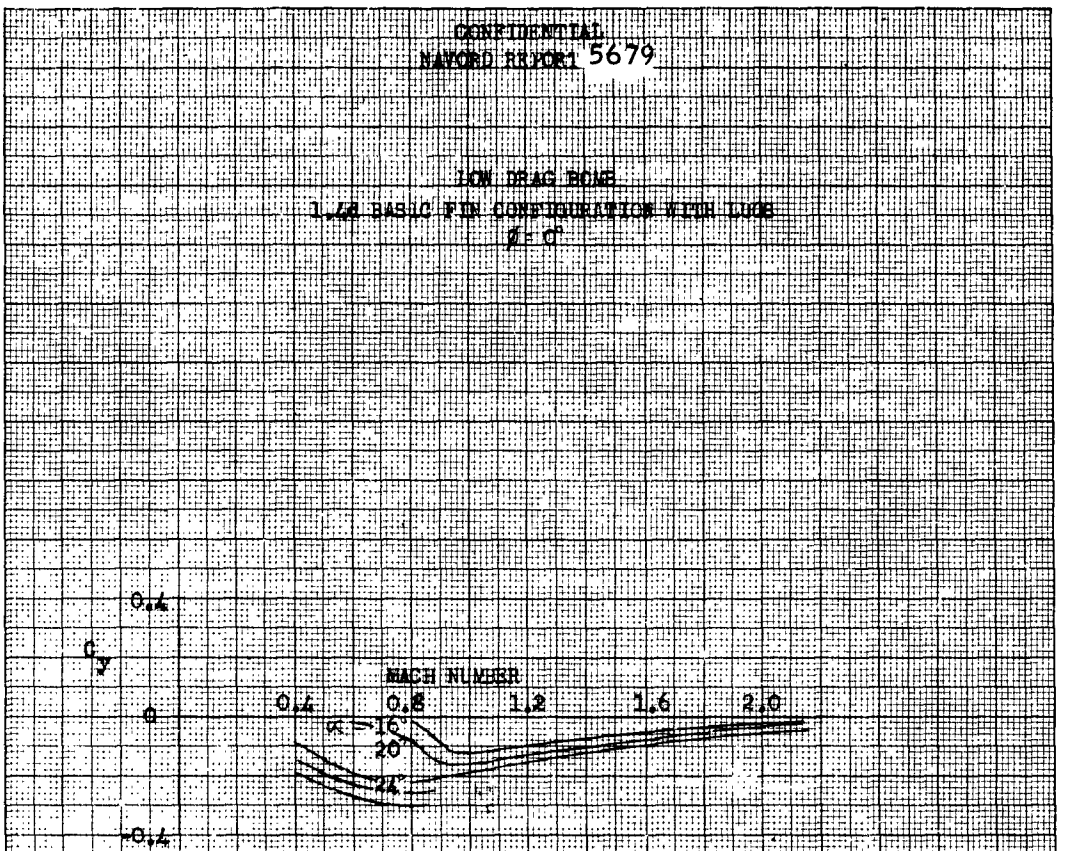

FIG. 22 SIDE FORCE COEFFICIENT, C_{y_α}, VERSUS MACH NUMBER FOR 0° FIN ORIENTATION

LOW DRAG BOMB
1.46 BASIC FIN CONFIGURATION WITH LUGS
$\phi = -22.5°$

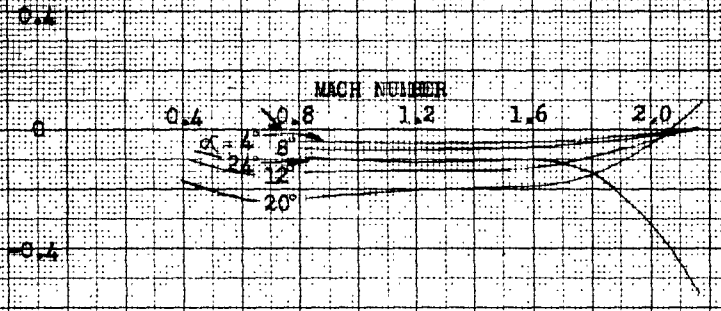

FIG. 23 SIDE FORCE COEFFICIENT, C_{y_s}, VERSUS MACH NUMBER FOR -22.5° FIN ORIENTATION

LOW DRAG BOMB
1.46 BASIC FIN CONFIGURATION WITH LUGS
$\phi = 45°$

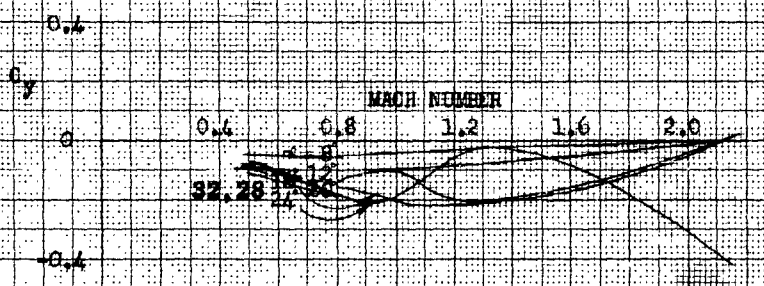

FIG. 24 SIDE FORCE COEFFICIENT, C_y, VERSUS MACH NUMBER FOR 45° FIN ORIENTATION

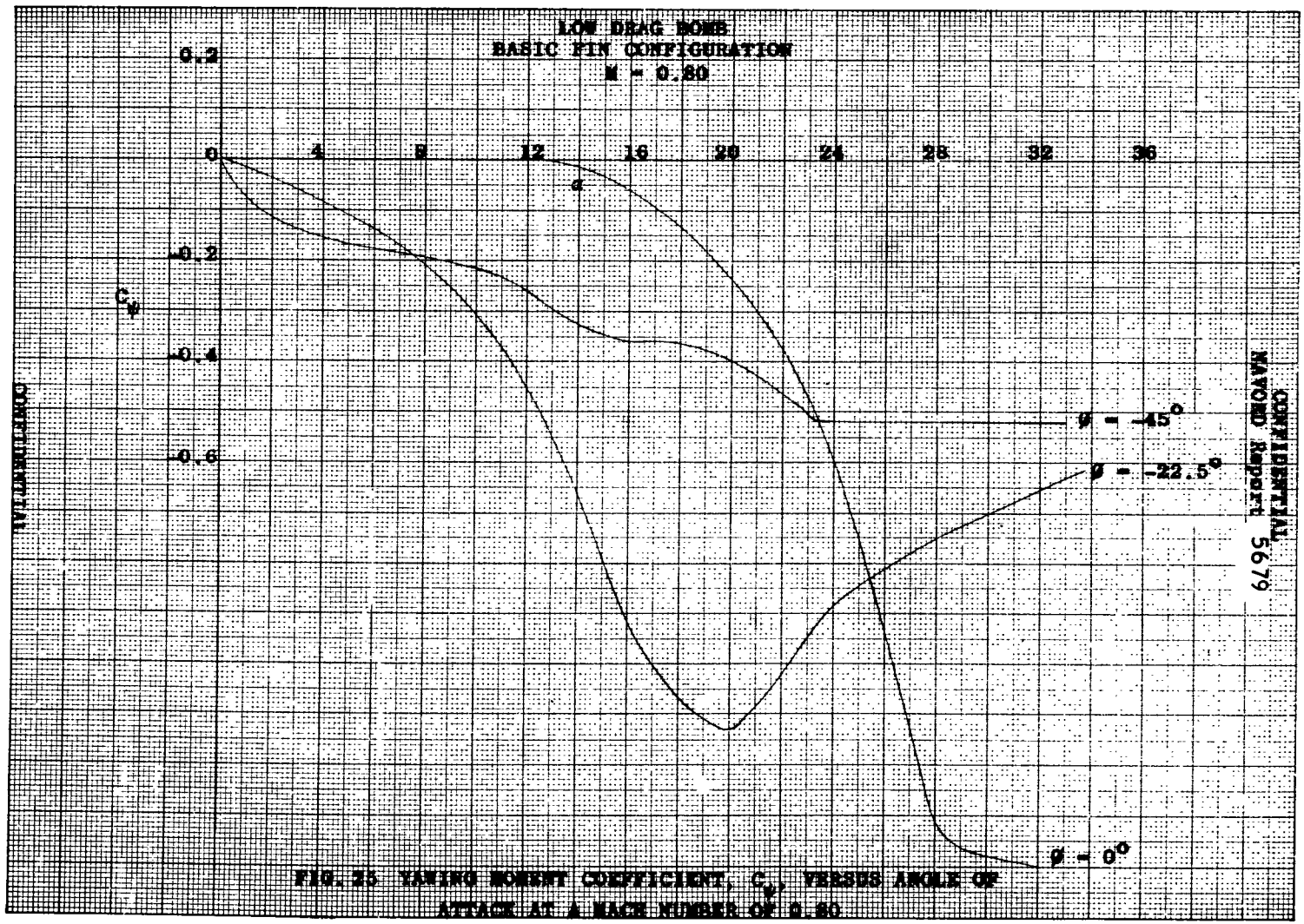

FIG. 25 YAWING MOMENT COEFFICIENT, C_ψ, VERSUS ANGLE OF ATTACK AT A MACH NUMBER OF 0.80

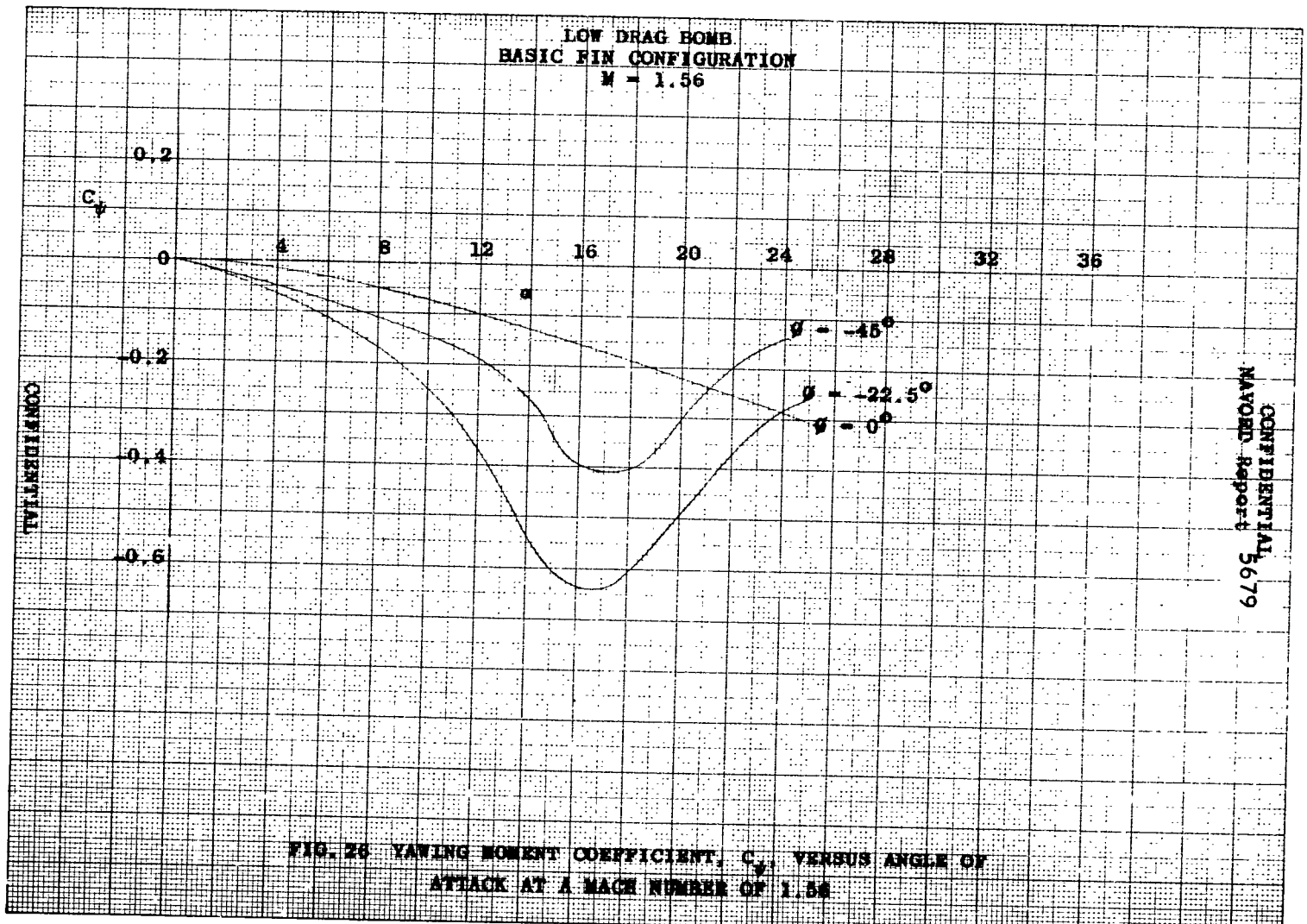

FIG. 26 YAWING MOMENT COEFFICIENT, C_ψ, VERSUS ANGLE OF ATTACK AT A MACH NUMBER OF 1.56

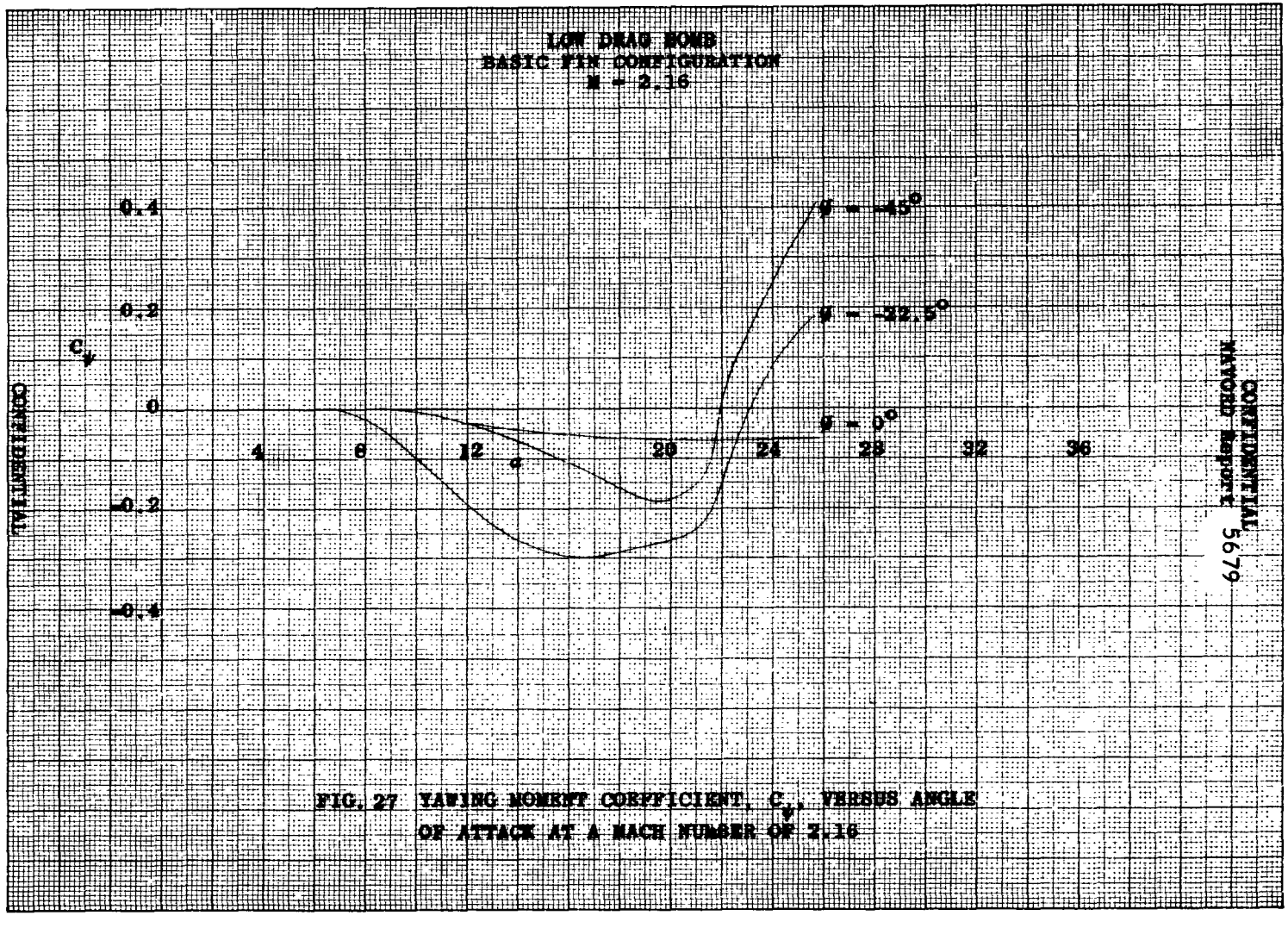

FIG. 27 YAWING MOMENT COEFFICIENT, C_{n_ψ}, VERSUS ANGLE OF ATTACK AT A MACH NUMBER OF 2.16

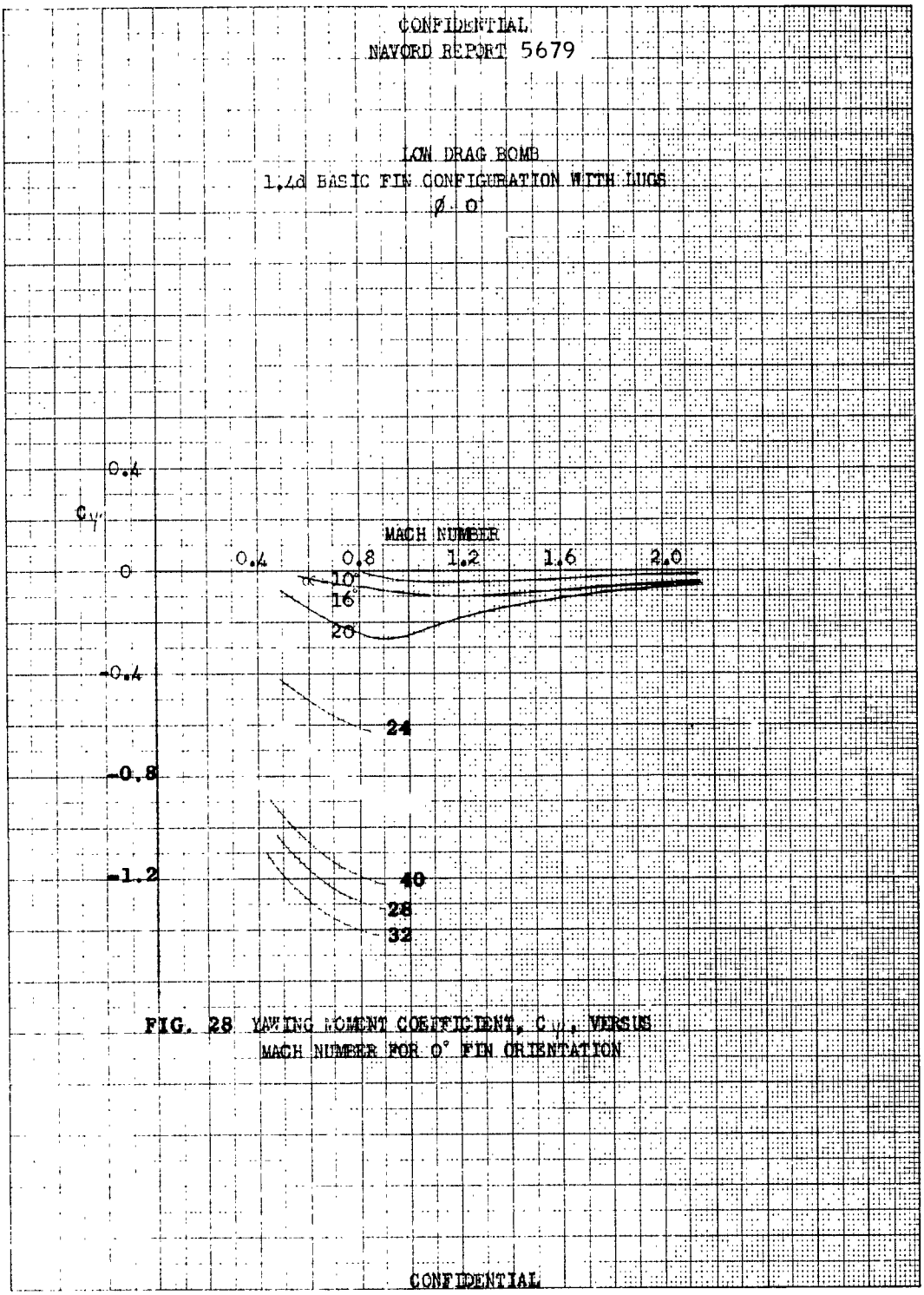

FIG. 28 YAWING MOMENT COEFFICIENT, $C_{y'}$, VERSUS MACH NUMBER FOR 0° FIN ORIENTATION

LOW DRAG BOMB
1.4d BASIC FIN CONFIGURATION WITH LUGS
$\phi = -22.5$

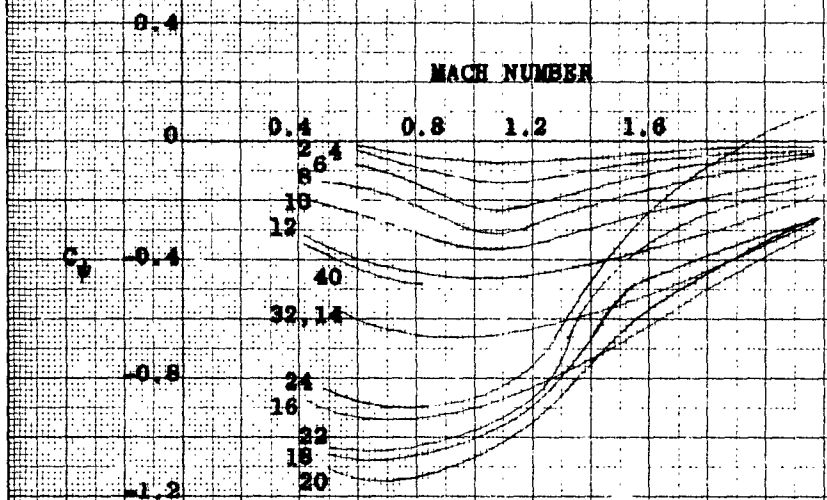

FIG. 29 YAWING MOMENT COEFFICIENT, C_{ψ}, VERSUS MACH NUMBER FOR -22.5° FIN ORIENTATION

LOW DRAG BOMB
1.4A BASIC FIN CONFIGURATION WITH LUGS
$\phi = -45°$

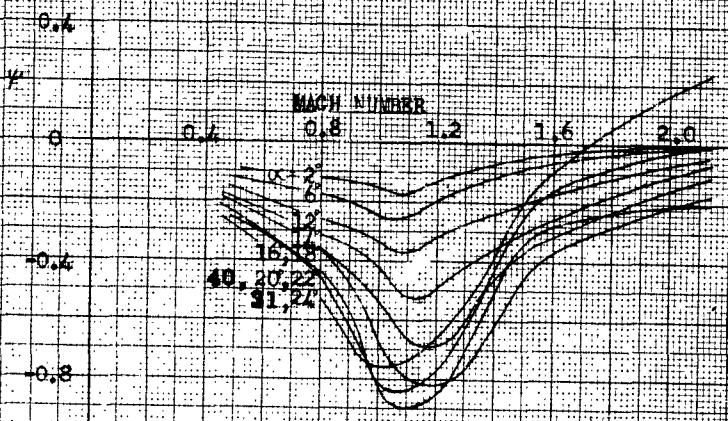

FIG. 30 YAWING MOMENT COEFFICIENT, C_{y_ψ}, VERSUS MACH NUMBER FOR -45° FIN ORIENTATION

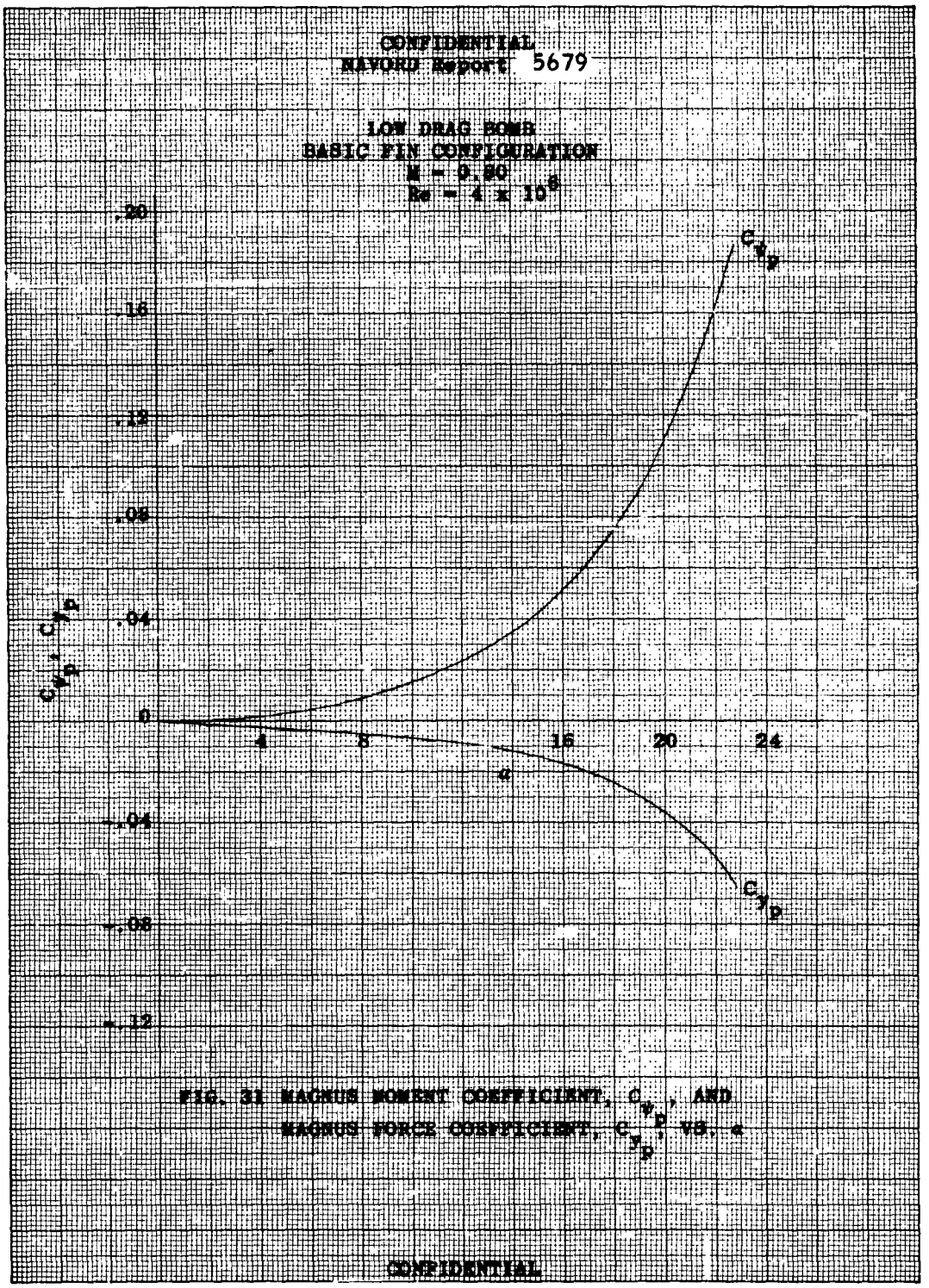

FIG. 31 MAGNUS MOMENT COEFFICIENT, C_{n_p}, AND MAGNUS FORCE COEFFICIENT, C_{y_p}, VS. α

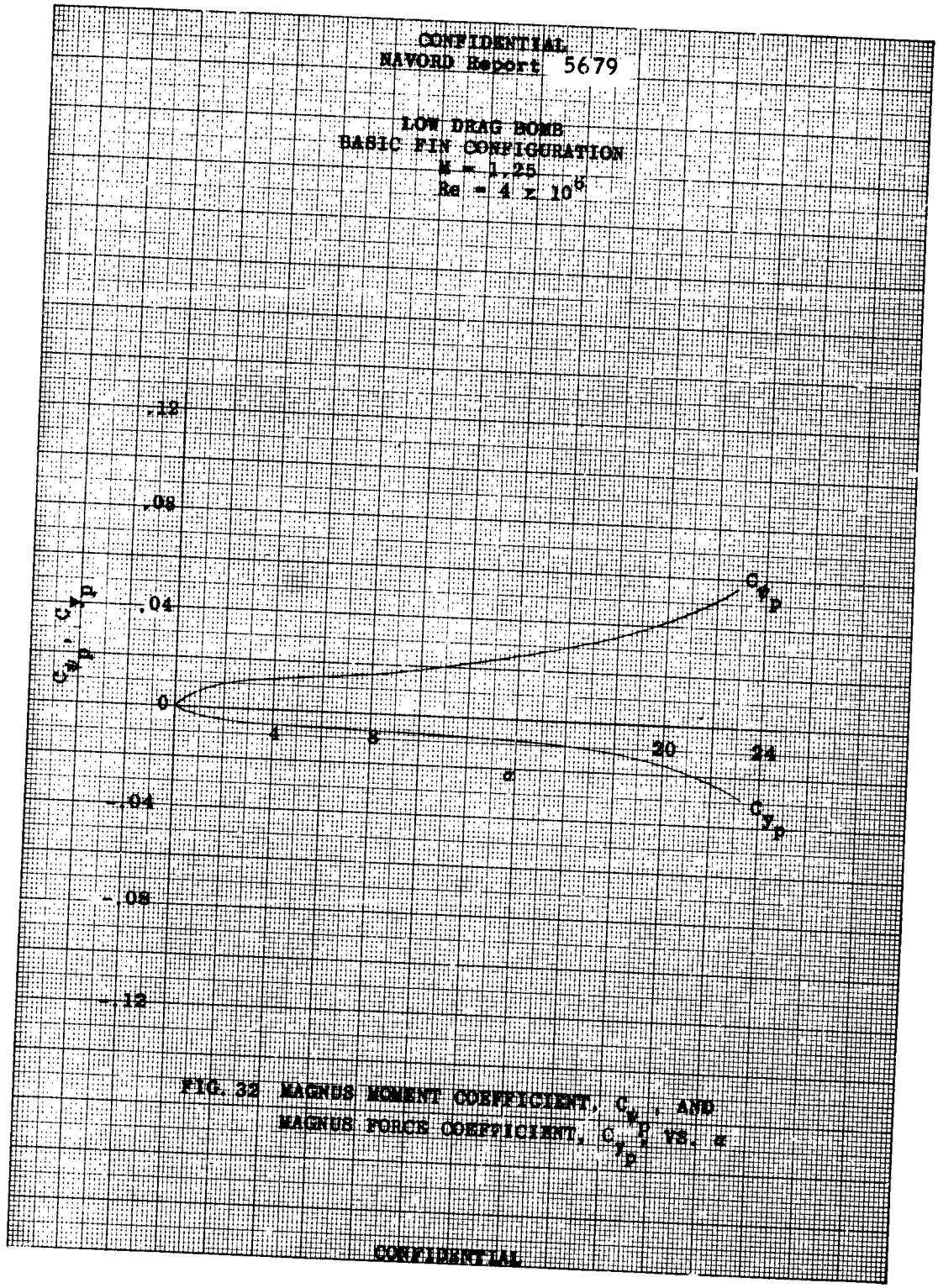

FIG. 32 MAGNUS MOMENT COEFFICIENT, C_{ϕ_p}, AND MAGNUS FORCE COEFFICIENT, C_{y_p}, VS. α

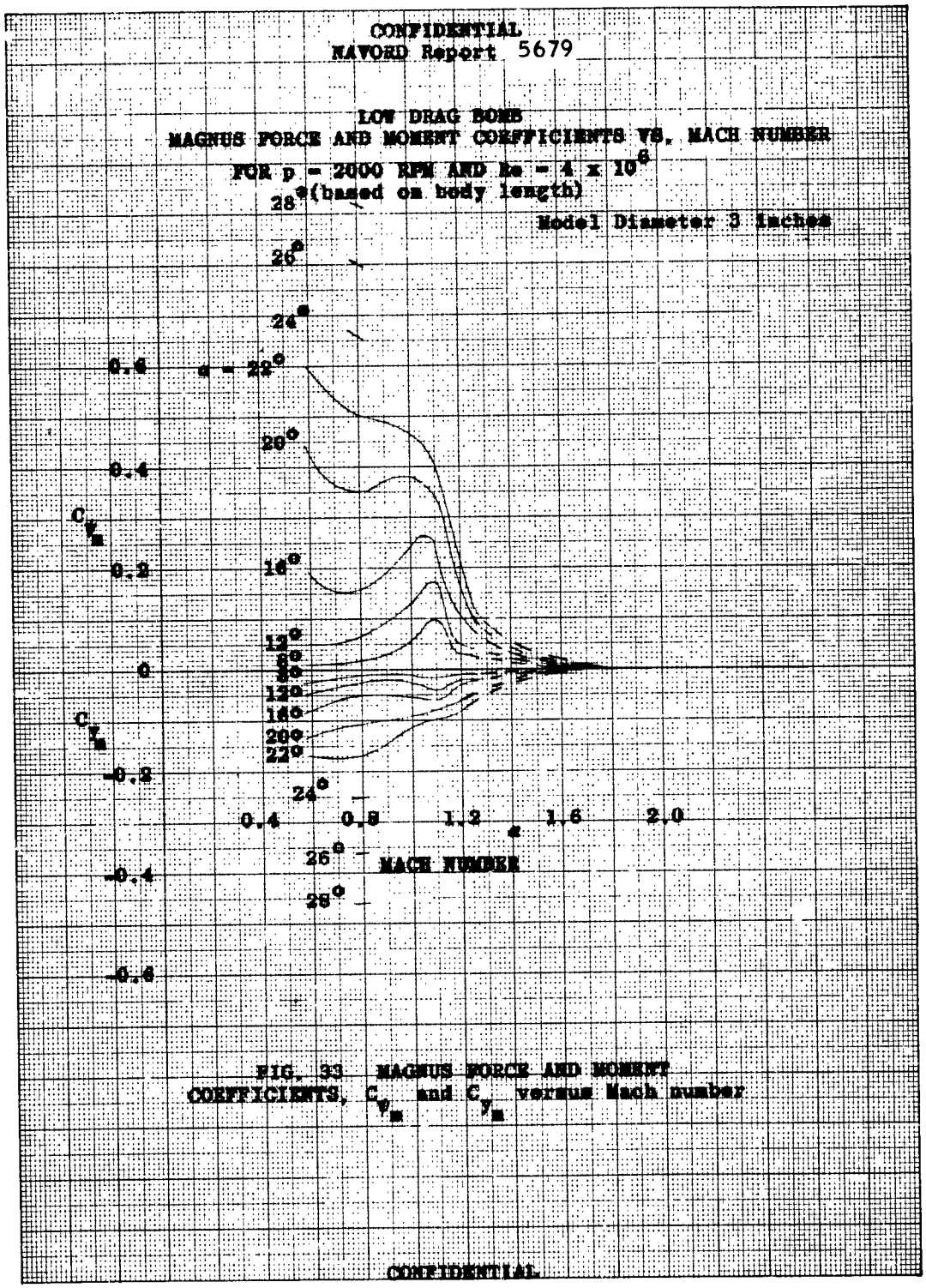

FIG. 33 MAGNUS FORCE AND MOMENT COEFFICIENTS, C_{y_m} and C_{y_m} versus Mach number

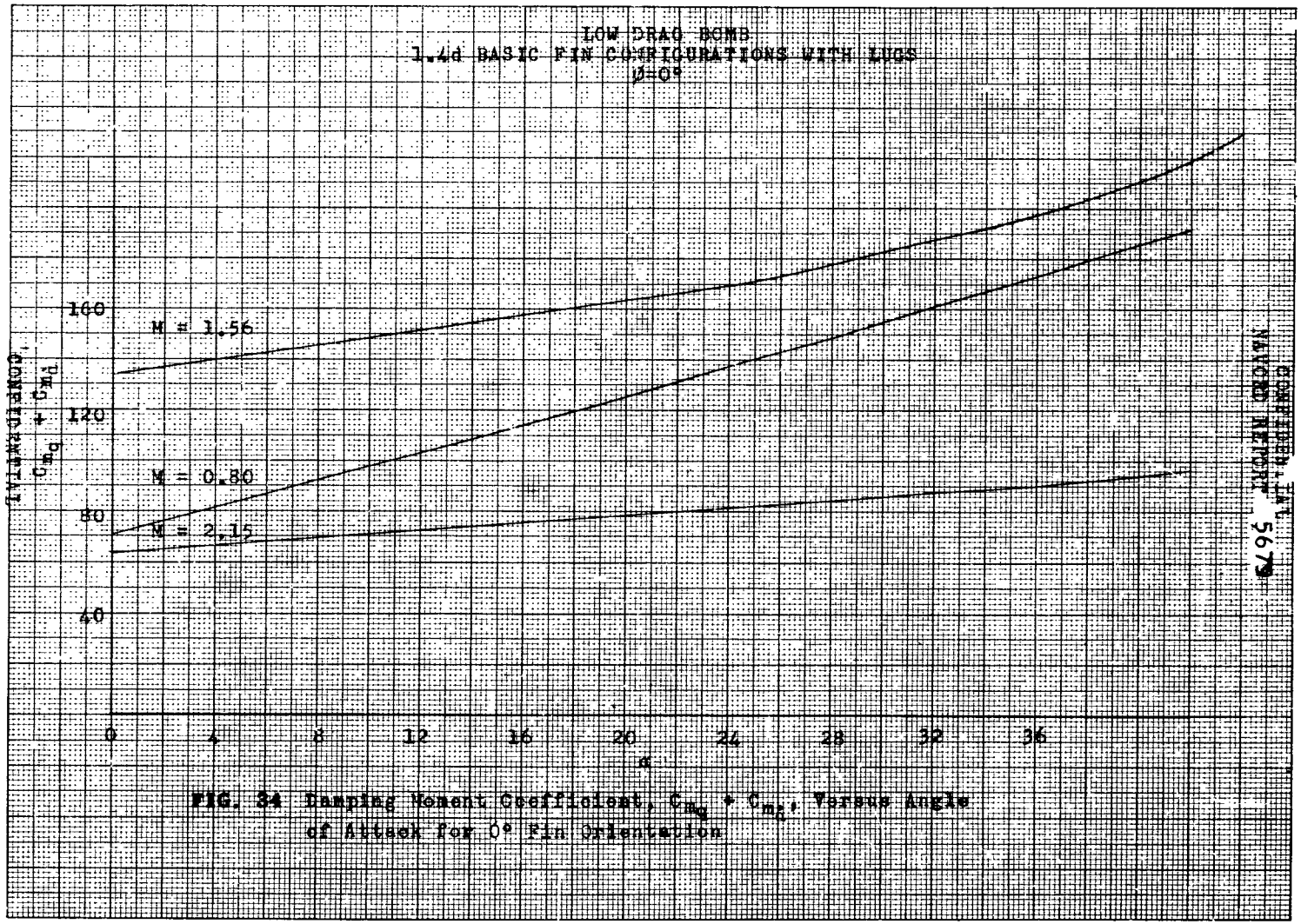

FIG. 34 Damping Moment Coefficient, $C_{m_q} + C_{m_{\dot{\alpha}}}$, Versus Angle of Attack for 0° Fin Orientation

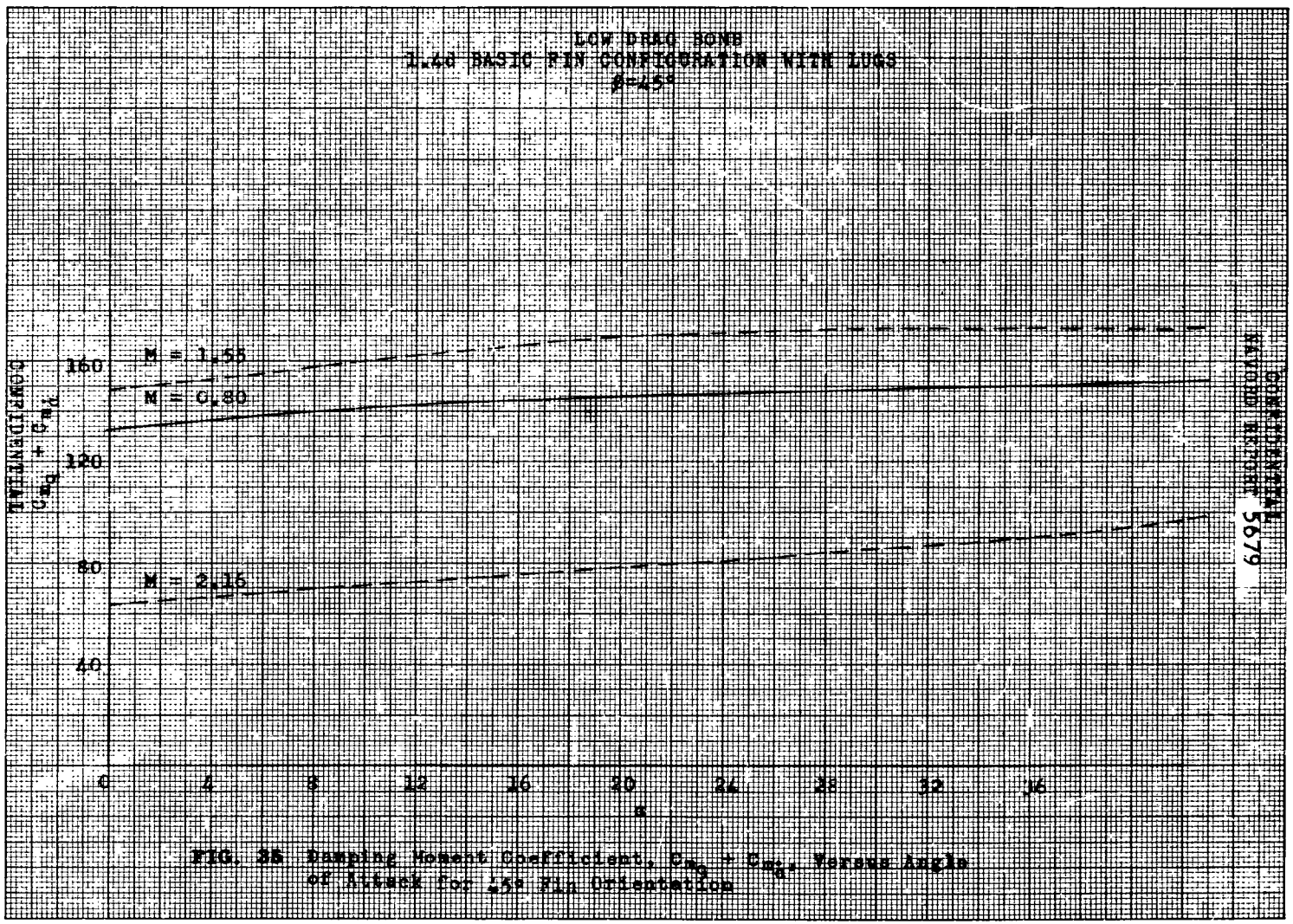

FIG. 35 Damping Moment Coefficient, $C_{m_q} + C_{m_{\dot{\alpha}}}$, Versus Angle of Attack for 45° Fin Orientation

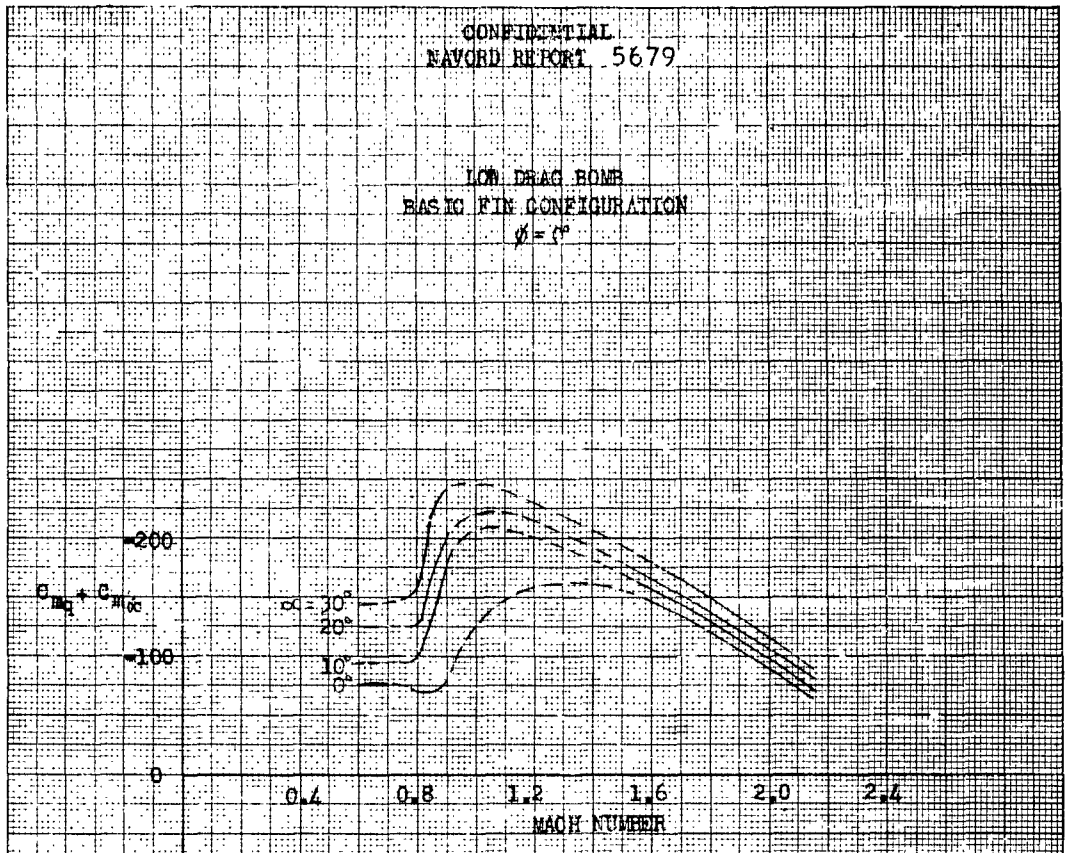

FIG. 36 DAMPING MOMENT COEFFICIENT, $C_{m_q} + C_{m_{\dot{\alpha}}}$ VERSUS MACH NUMBER

FIG. 27 PITCHING MOMENT COEFFICIENT, $C_{m_{c/4}}$

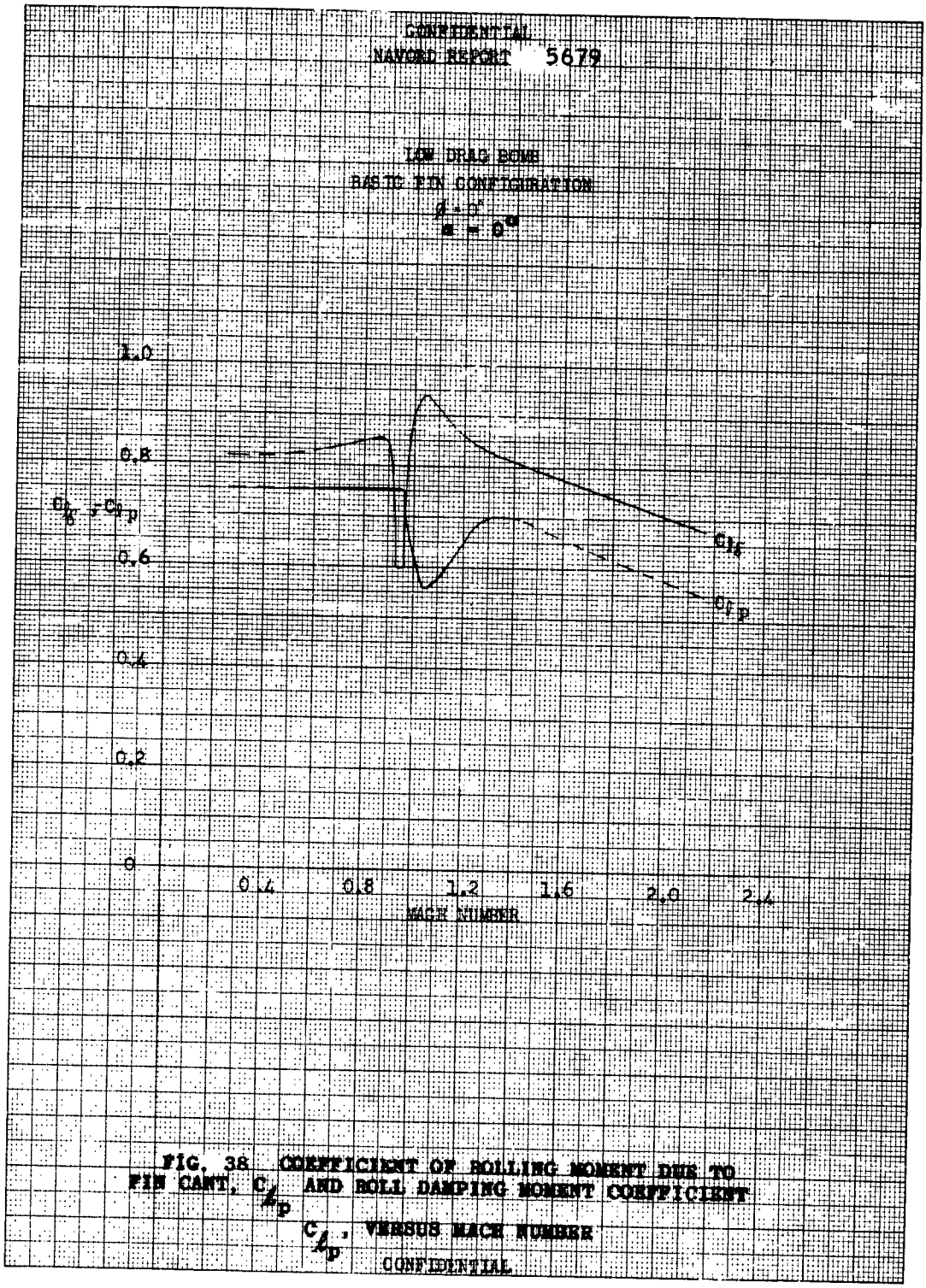

FIG. 38 COEFFICIENT OF ROLLING MOMENT DUE TO FIN CANT, C_{l_δ} AND ROLL DAMPING MOMENT COEFFICIENT C_{l_p}, VERSUS MACH NUMBER

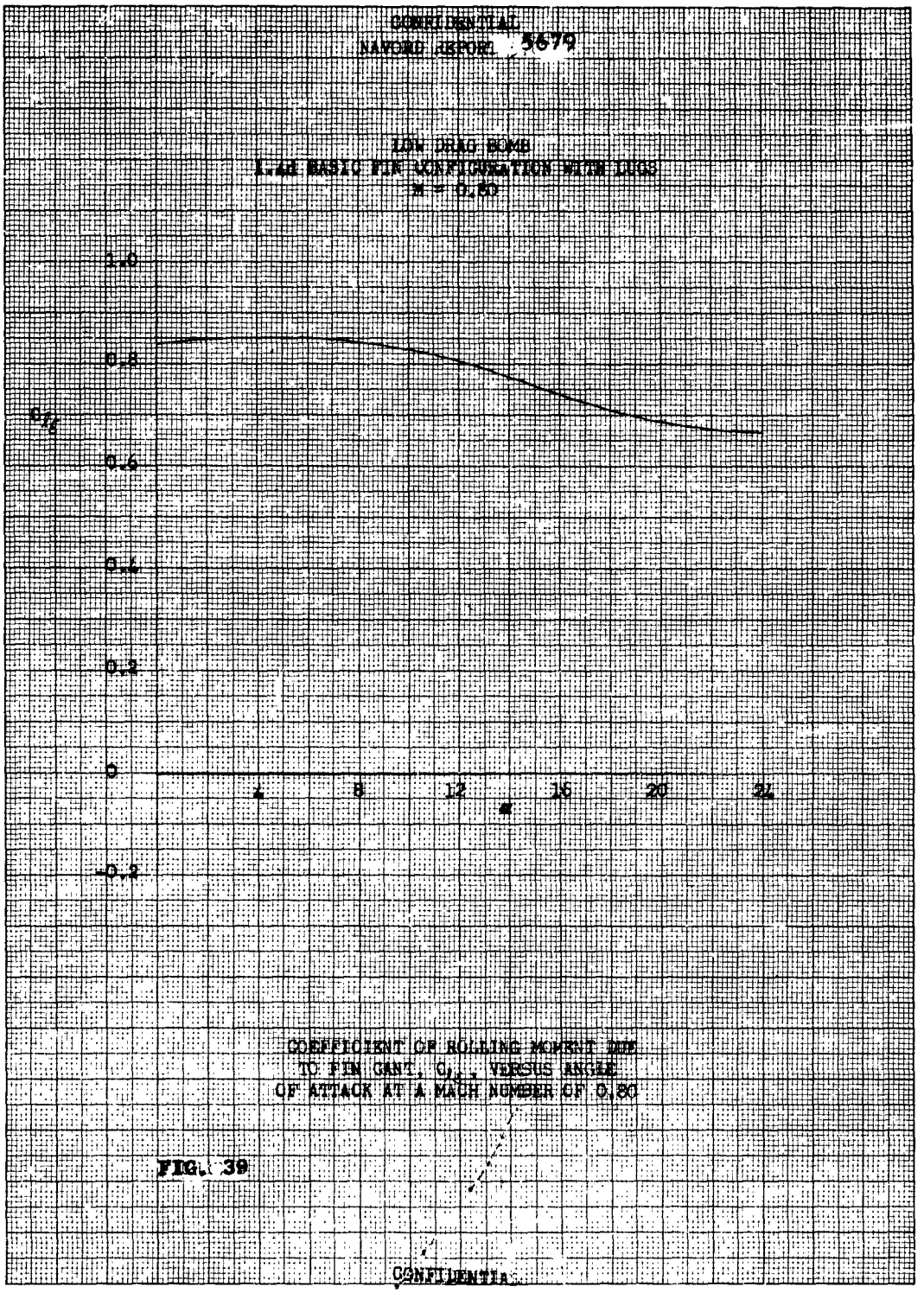

COEFFICIENT OF ROLLING MOMENT DUE TO FIN CANT, C_{l_δ}, VERSUS ANGLE OF ATTACK AT A MACH NUMBER OF 0.80

FIG. 39

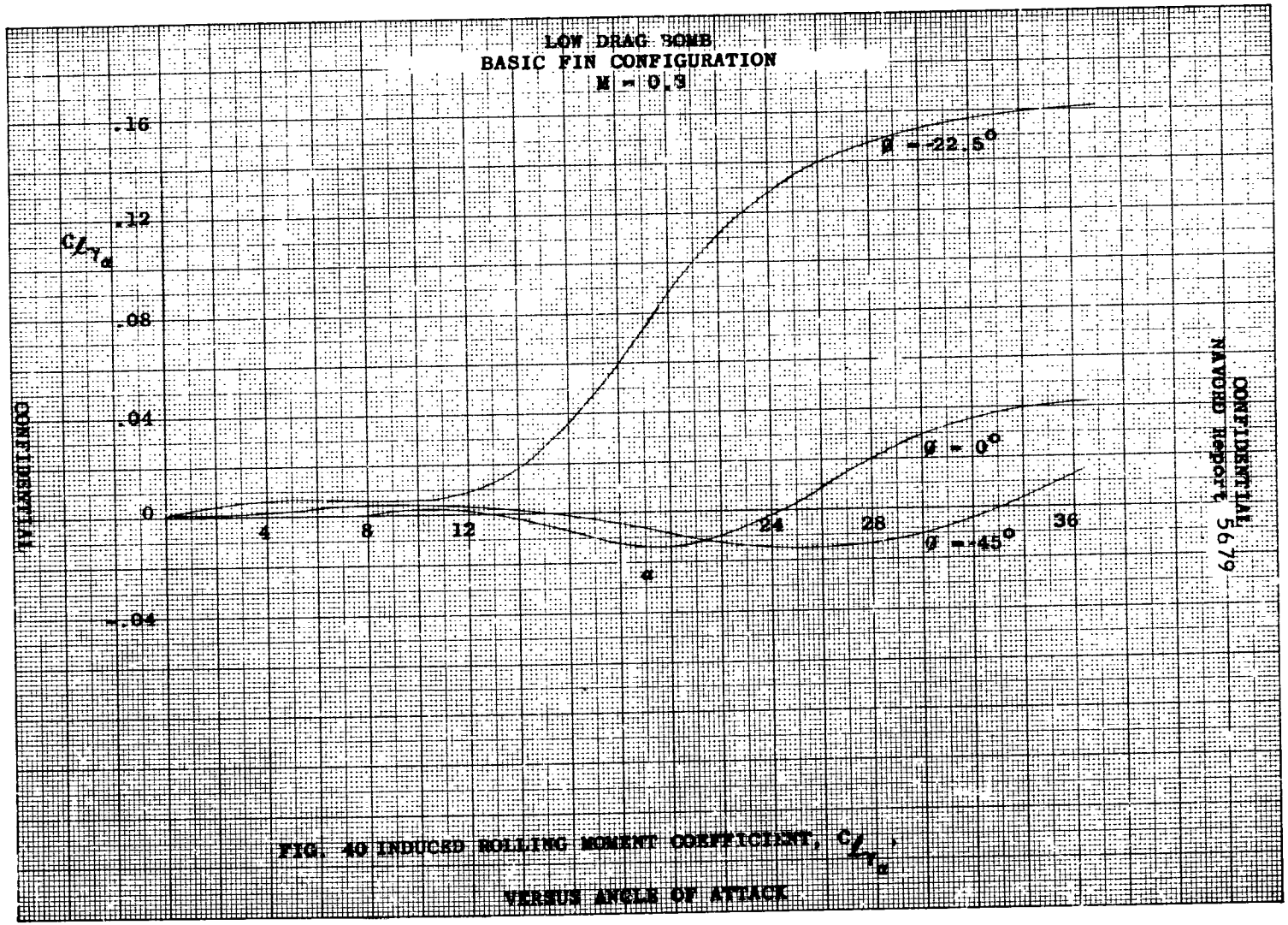

FIG. 40 INDUCED ROLLING MOMENT COEFFICIENT, $C_{\ell_{\gamma_\alpha}}$, VERSUS ANGLE OF ATTACK

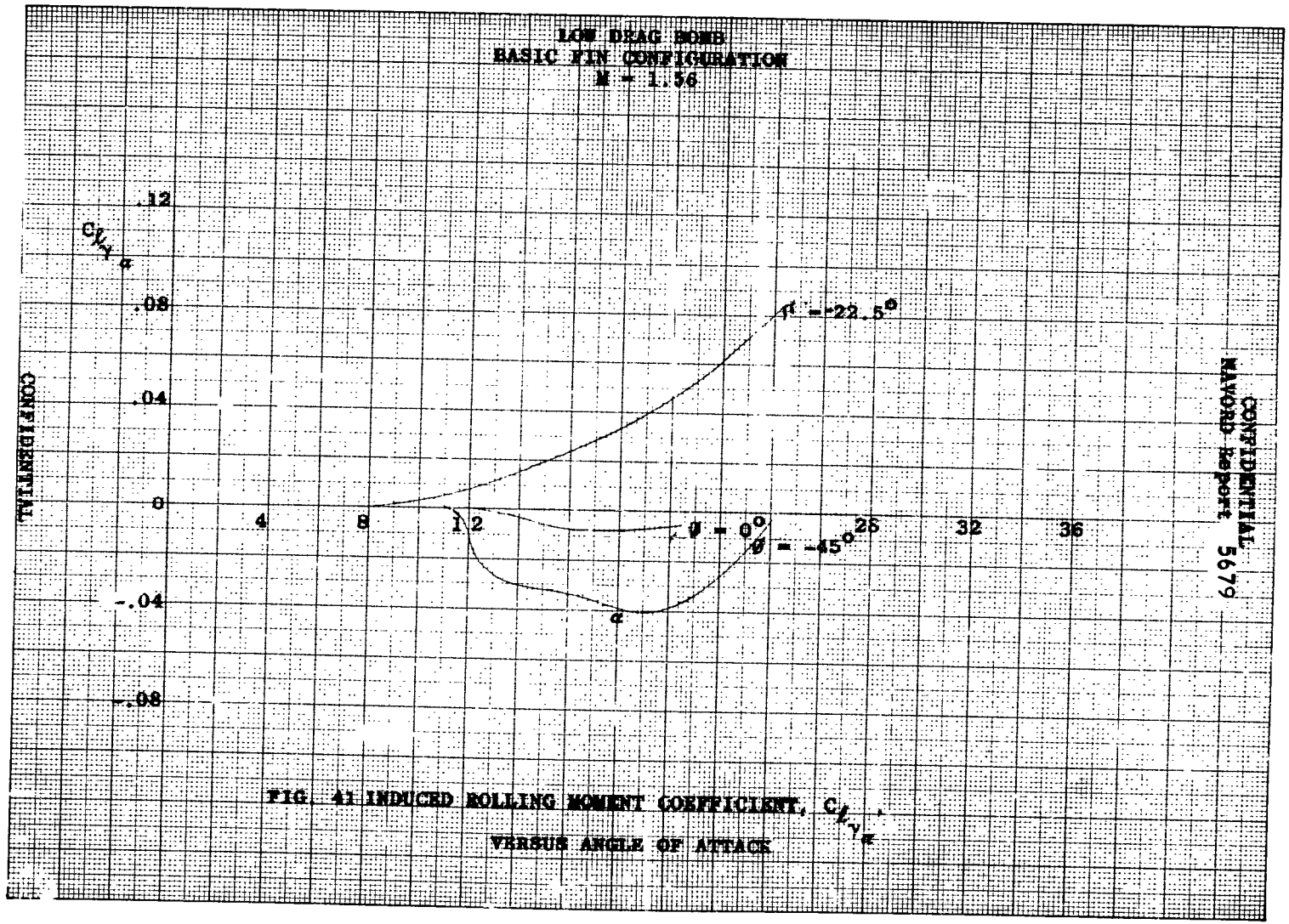

FIG. 41 INDUCED ROLLING MOMENT COEFFICIENT, $C_{l_{\gamma_\alpha}}$, VERSUS ANGLE OF ATTACK

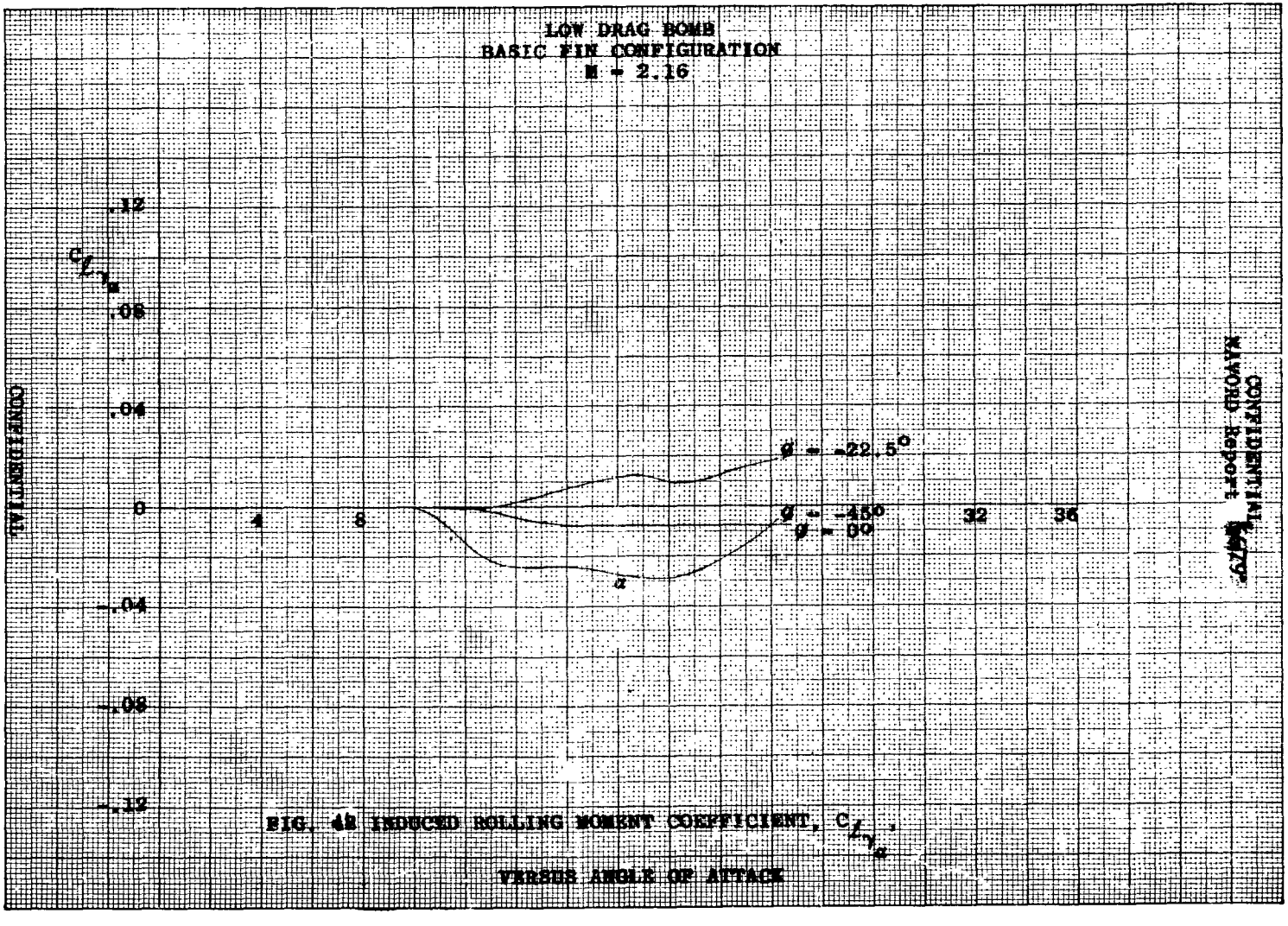

FIG. 42 INDUCED ROLLING MOMENT COEFFICIENT, $C_{l_{\gamma_a}}$, VERSUS ANGLE OF ATTACK

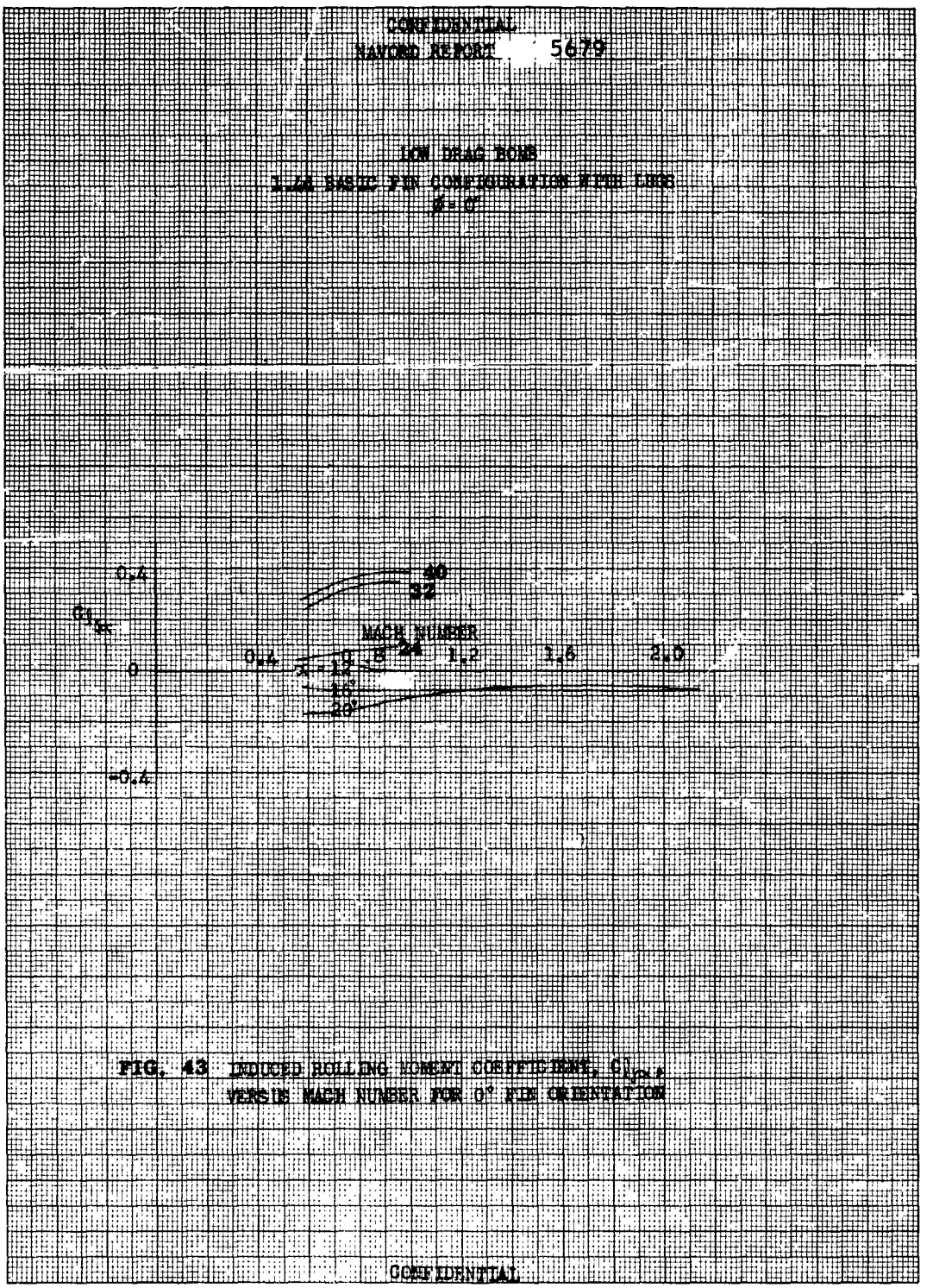

FIG. 43 INDUCED ROLLING MOMENT COEFFICIENT, $C_{l_{\delta_R}}$, VERSUS MACH NUMBER FOR 0° FIN ORIENTATION

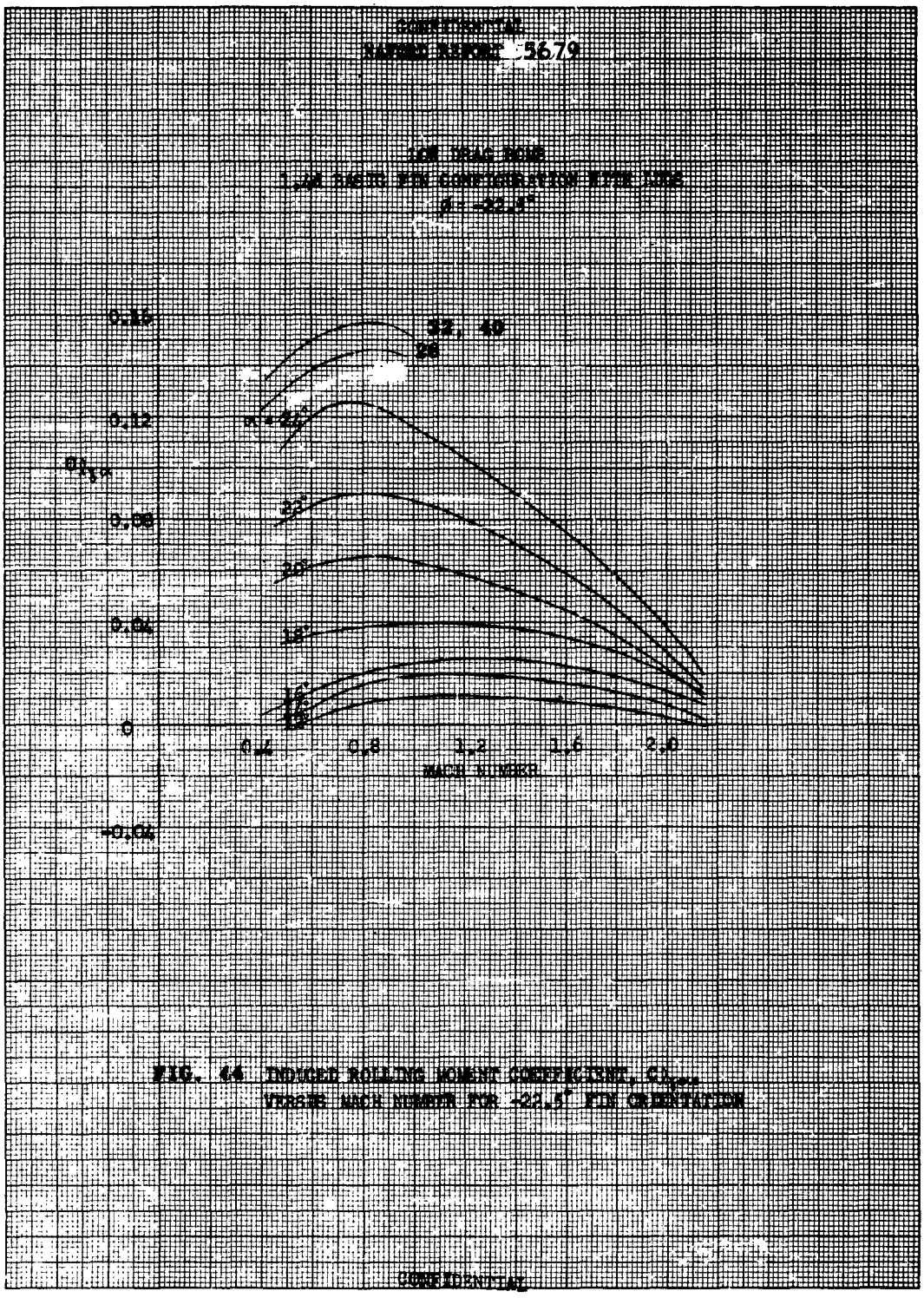

FIG. 44 INDUCED ROLLING MOMENT COEFFICIENT, $C_{l_{\phi_1}}$, VERSUS MACH NUMBER FOR -22.5° FIN ORIENTATION

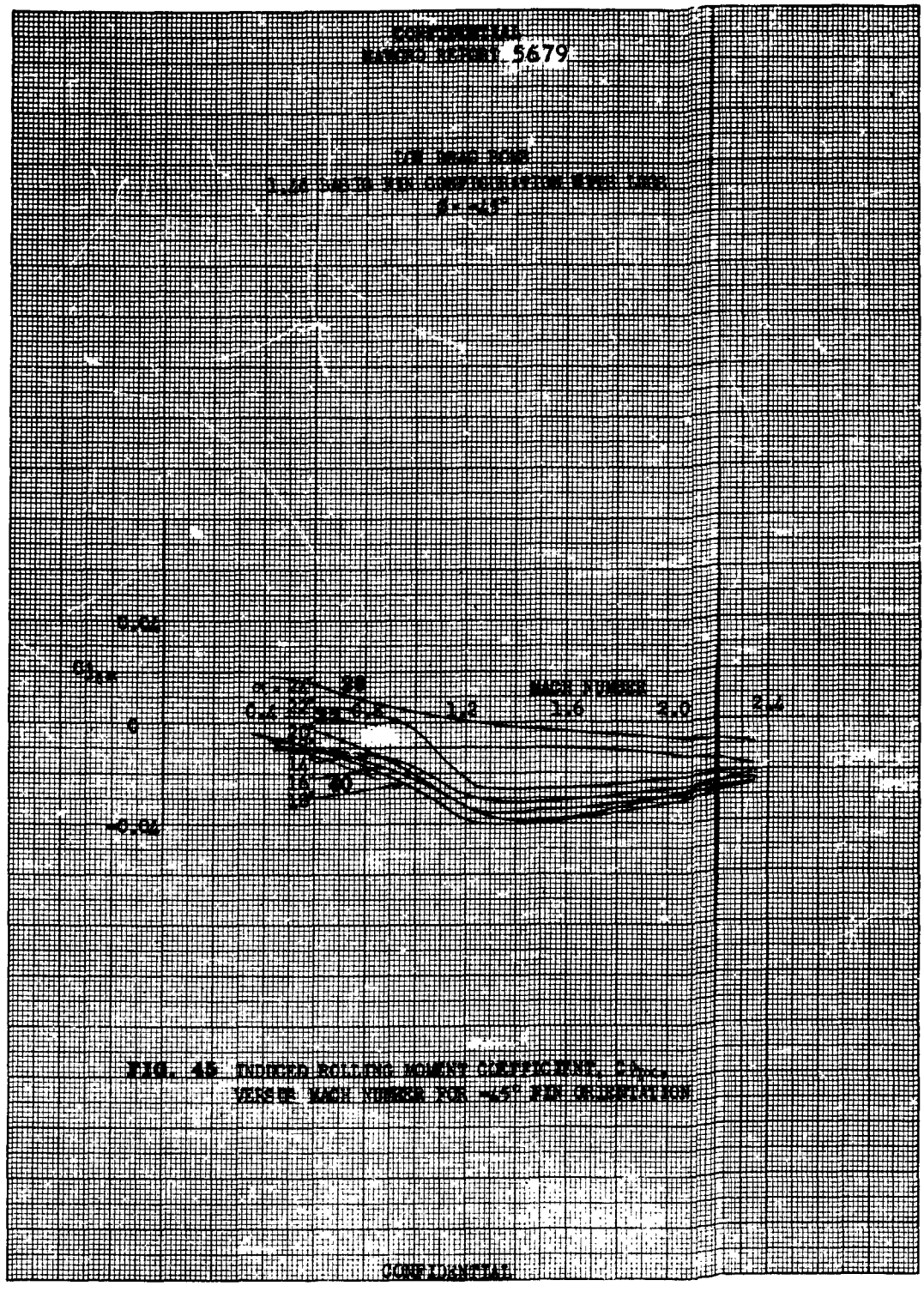

FIG. 45 INDUCED ROLLING MOMENT COEFFICIENT, $C_{l_{\delta_a}}$, VERSUS MACH NUMBER FOR ±5° AIR DEFLECTION

Figure 48 - Zero-Yaw Drag Coefficient as a Function of Mach Number